Petroleum Science 23 (2026) 4204–4222

Contents lists available at ScienceDirect

Petroleum Science

journal homepage: www.keaipublishing.com/en/journals/petroleum-science

Original Paper

A three-dimensional fuzzy dynamic risk assessment model with dynamic cloud weights for human operational errors in oil and gas pipelines

Xue-Qiang Qu, Jiang-Tao Cao *, Tao-Yan Zhao **, Zhe Kan

School of Information and Control Engineering, Liaoning Petrochemical University, Fushun, 113001, Liaoning, China

ARTICLE INFO

Article history:
Received 26 June 2025
Received in revised form
10 November 2025
Accepted 27 January 2026
Available online 31 January 2026

Edited by Teng Zhu and Meng-Jiao Zhou

Keywords:
Dynamic risk assessment
Human operational error
Dynamic cloud weight
Data enhancement
Three-dimensional fuzzy matrix

ABSTRACT

Given the inherent complexity of human behavior, situational dependencies, and fragmented data, accurately assessing the risks arising from human operational errors in oil and gas pipelines remains a formidable challenge. To address these limitations, this study proposed a three-dimensional fuzzy dynamic risk assessment model with dynamic cloud weights (DW-TDFE). First, based on seven human operational errors, a risk assessment index system was established. Second, historical data (including accident frequency and casualty records) were utilized to determine initial indicator weights using the analytic hierarchy process (AHP). To simulate real-world disturbances, Gaussian noise was introduced. A combination of a time decay factor and a hyperbolic tangent function was employed to smooth fluctuations, yielding dynamic weights. Subsequently, data-driven dynamic membership functions were designed. Based on this, a data augmentation method was introduced to capture local trends in accident frequency and severity. These processes produced a three-dimensional fuzzy matrix, representing the temporal evolution of risk levels across assessment indicators. Finally, cloud models were incorporated to manage data uncertainty using the improved TOPSIS algorithm. Time decay and standard deviation corrections were introduced to optimize dynamic weight management. The DW-TDFE model achieves superior accuracy and reliability relative to conventional approaches. This study offers theoretical and practical references for the dynamic risk assessment of oil and gas pipelines.

1. Introduction

Oil and gas resources play a pivotal role in economic development. Pipeline transportation has become the primary mode for their global distribution. As of early 2022, the total length of planned or under-construction oil and gas pipelines worldwide reached approximately 166,000 km. Compared to road and rail transportation, pipeline systems offer notable advantages in terms of high transport capacity and energy efficiency. However, according to a report on the Pipeline and Hazardous Materials Safety Administration (PHMSA), human operational errors remain a major contributor to pipeline accidents (PHMSA, 2023). Such errors are inherently linked to human activities, characterized by significant uncertainty. To ensure safe pipeline operations, it is essential to develop preventive measures and targeted control strategies (Lawal and Afolalu, 2024).

Bayesian networks are commonly utilized in dynamic risk assessment of oil and gas pipelines, modeling the probabilistic dependencies among risk factors. These networks integrate real-time observational data with prior knowledge, allowing for the continuous updating of state probabilities and facilitating quantitative analysis and trend prediction. Aulia et al. (2021) and Cui et al. (2020) developed a risk assessment model based on dynamic Bayesian networks, which combines fault tree analysis and finite element methods. This model consolidates historical data with real-time observations to dynamically update probability distributions. It provides a quantitative framework for lifecycle risk assessment under third-party interference. Roberto et al. (2020) combined Bayesian networks with safety barrier

* Corresponding author.
** Corresponding author.
E-mail addresses: jtcao@lnpu.edu.cn (J.-T. Cao), zhaotaoyan@lnpu.edu.cn (T.-Y. Zhao).
Peer review under the responsibility of China University of Petroleum (Beijing).

https://doi.org/10.1016/j.petsci.2026.01.044

evaluation to simulate risk scenarios for the Goliat oil platform in the Barents Sea, Norway. This approach demonstrated its effectiveness in accident prevention and risk management in the Arctic environment. Despite these advancements, these models face challenges in managing real-time temporal dependencies. As system states and variable relationships evolve, maintaining network structures and performing probabilistic inference becomes increasingly computationally complex, which can further degrade model stability.

The analytic hierarchy process (AHP) (Díaz et al., 2022) is widely utilized to decompose complex systems into hierarchical structures. Saffarian et al. (2020) developed a fuzzy-AHP approach for the environmental risk assessment of gas-fired power plants, thereby improving the treatment of uncertainties. Zhan et al. (2025) combined AHP with the entropy weight method (EWM) to establish an evaluation system encompassing fifteen geological, hydrological, and human factors. By integrating with remote sensing and geographic information technology, the system successfully assessed urban ground-subsidence risk in Shanghai. However, traditional AHP relies heavily on expert judgment for determining indicator importance, making the judgment matrix susceptible to subjective bias. Furthermore, the fixed weights derived from AHP cannot accommodate the dynamic fluctuations of pipeline risk factors.

The high degree of uncertainty associated with human operational errors complicates the extraction of critical information from risk data. To improve risk assessment accuracy, data enhancement is essential. Riela (2022) developed an approach integrating data augmentation, machine learning, and visual analytics to address missing data, oversample minority classes, and model causal relationships. This approach effectively enhances risk prediction performance for hospital-acquired infections in ICU patients. Pezoulas et al. (2021) introduced a workflow combining data quality control, virtual population generation, and hybrid machine learning. By generating high-quality virtual data to augment real clinical datasets, this workflow significantly improves risk stratification accuracy. Fahd and Miah (2023) integrated data augmentation with a deep learning model based on multilayer perceptrons. This strategy effectively mitigated issues associated with small dataset size and class imbalance, thus improving risk prediction performance. However, these enhanced datasets may fail to fully capture real-time variations in human operational errors.

The cloud model integrates ambiguity and uncertainty through expectation, entropy, and hyper-entropy. Expectation reflects the central tendency of a concept; entropy quantifies the degree of ambiguity and uncertainty associated with that concept (higher values indicating greater ambiguity and uncertainty); hyper-entropy represents the uncertainty of variability of entropy itself, capturing the uncertainty of the ambiguity. By treating membership degrees as fuzzy variables, the cloud model effectively represents human judgment errors, enabling the rapid conversion between qualitative concepts and quantitative data. This facilitates a more comprehensive quantification of the randomness of risk factors and the ambiguity of the severity of their consequences. Yu et al. (2021) proposed a risk-matrix method based on the cloud model. This approach integrates entropy and hyper-entropy to quantify fuzziness and randomness. By enhancing the Mamdani inference algorithm and the centroid method, this approach demonstrated superior performance in addressing uncertainty in practical applications. Li et al. (2020) developed an improved failure mode and effects analysis method integrating the cloud model with the best-worst method. This strategy leverages the cloud model to handle fuzziness and randomness, incorporates dynamic expert weight allocation, and considers maintenance costs and time factors, thereby providing a more comprehensive and accurate risk assessment. Lin et al. (2020) introduced a tunnel-construction risk assessment method based on an enhanced cloud model. This method incorporated fuzziness and randomness into the RMPM risk indicator system and combined AHP with forward/reverse cloud generators, thus improving evaluation reliability. However, the application of the cloud model in dynamic risk assessments remains challenging due to computational complexity and high sensitivity to parameter variations.

The technique for order preference by similarity to an ideal solution (TOPSIS) method can effectively handle quantitative and qualitative indicators. It allows for flexible integration of criterion weights, enabling a precise representation of their relative importance, and favors compromise solutions that avoid significant weaknesses. TOPSIS generates a closeness coefficient ranging from 0 to 1, facilitating a comprehensive ranking of alternatives. For risk assessment, each indicator's priority is determined by its Euclidean distance from the positive and negative ideal solutions. Indicators are ranked according to their relative closeness to the ideal solution. Koulinas et al. (2021) proposed a framework that integrates TOPSIS with a risk matrix and Monte Carlo simulation to assess project schedule risks, demonstrating its effectiveness in predicting project completion probabilities and optimizing risk management decisions. Gul et al. (2021) integrated TOPSIS into occupational risk assessment for the manufacturing industry, proving its superiority in managing uncertainties and prioritizing risks in practical applications. Pathan et al. (2022) applied AHP, TOPSIS, and GIS in flood-risk assessment. The study found that TOPSIS outperformed AHP in prediction accuracy and identification of high-risk areas requiring intervention. However, TOPSIS exhibits limitations in dynamic contexts due to static weight allocation and inadequate adaptability to evolving risk factors.

Existing dynamic Bayesian network models (Aulia et al., 2021; Cui et al., 2020; Roberto et al., 2020) demonstrate limited capability for handling complex real-time dependencies, while data-enhancement techniques (Riela, 2022; Pezoulas et al., 2021; Fahd and Miah, 2023) may compromise model generalization. The cloud model (Yu et al., 2021; Li et al., 2020; Lin et al., 2020) faces parameter sensitivity issues, and the TOPSIS algorithm (Koulinas et al., 2021; Gul et al., 2021; Gul et al., 2021, 2021) lacks dynamic adaptability. To address these challenges, this study proposed a three-dimensional fuzzy dynamic risk assessment model incorporating dynamic cloud weights (DW-TDFE). Gaussian noise was introduced to simulate real-world disturbances. The model combined entropy-based uncertainty quantification with a time decay factor to control weight fluctuations. A hyperbolic tangent function further compressed the amplitude of weight fluctuations, enhancing model stability under noisy conditions. Additionally, based on sliding-window summation, a time-series data enhancement method was proposed, incorporating mirror padding to address data boundary issues. This improves the representation of local trends, smooths short-term fluctuations, and captures the characteristics of medium- and long-term risks.

To capture risk evolution, a three-dimensional fuzzy matrix was constructed, encompassing risk assessment indicators, risk levels, and time points. Furthermore, the model integrated cloud models with the TOPSIS algorithm to address the uncertainty and ambiguity in risk assessment indicators, thereby enhancing model performance. Compared to the static expert-evaluation-based model proposed by Wang et al. (2023), the DW-TDFE model demonstrates superior long-term reliability and adaptability to persistent disturbances and sparse data. Additionally, it generated a spatiotemporal multidimensional heatmap of risk levels, offering a realistic depiction of risk evolution that aligns with practical management needs. Relative to the improved AHP-TOPSIS model proposed by Wang and Duan (2019), the DW-TDFE model effectively mitigates ambiguity. While the AHP-TOPSIS model relies on normalized raw data, the DW-TDFE model integrates an enhanced TOPSIS method with cloud models to quantify ambiguity and uncertainty via entropy and hyper-entropy. It employs a sliding-window summation method, which attenuates the distortion of long-term trends by short-term risk fluctuations. The dynamic Bayesian network model proposed by Bakhtiari et al. (2025) requires high-dimensional probabilistic inference and imposes considerable computational overhead. By comparison, the DW-TDFE model employs dynamic weights and an improved TOPSIS algorithm to determine risk priorities. This streamlined design makes the DW-TDFE model more efficient and better suited for real-time monitoring of oil and gas pipeline risks.

The primary contributions of this study are as follows: (1) A risk assessment indicator system was developed based on historical pipeline accident data, ensuring alignment with real-world operational conditions. (2) The initial weights of indicators were determined using the AHP. Gaussian noise was introduced to simulate real-world disturbances, and uncertainty was quantified via the standard deviation of the weights. A dynamic weight adjustment matrix was developed by incorporating a time decay factor. Additionally, a hyperbolic tangent function was applied to suppress excessive weight fluctuations and generate stable dynamic weights. (3) Data-driven dynamic membership functions were designed. The parameters were optimized using a gradient descent algorithm under a maximum log-likelihood framework. A time-series data enhancement method was proposed based on sliding-window accumulation to jointly extract features from accident frequency and casualty data. Mirror-symmetric padding was applied at data boundaries to improve continuity and prevent information loss. A three-dimensional fuzzy matrix of risk indicators, risk levels, and time periods was constructed. The time-varying risk levels of indicators were illustrated through heatmaps. (4) The cloud model was integrated with the improved TOPSIS algorithm to enable dynamic risk ranking. A time decay factor and a standard deviation correction term were incorporated to increase robustness against noise and sensitivity to risk dynamics. (5) Adaptive risk assessment was achieved by dynamically balancing weight fluctuations induced by Gaussian noise. This ensured both stability and responsiveness to evolving risks. (6) The DW-TDFE model was applied to oil and gas systems and benchmarked against a Bayesian dynamic risk assessment model. The results demonstrate that the DW-TDFE model outperforms the Bayesian model in terms of temporal stability and risk differentiation.

In the remainder of this paper, Section 2 introduces the theoretical foundations and methods of risk assessment. Section 3 details the construction of the DW-TDFE model. Section 4 validates the model's performance in a case study. Finally, Section 5 draws the conclusions.

2. Risk assessment theories and methods

2.1. AHP

AHP is widely employed to determine indicator weights. It primarily includes four steps (Ba et al., 2021):

(1) Establishing a hierarchical model.
(2) Constructing a judgment matrix: The importance of each indicator for the j-th object is quantified using a 5-point scale. Each indicator's contribution to the overall decision is represented as a proportion, forming a judgment matrix $\mathbf{R}$ for pairwise comparisons among the m_j indicators of the j-th object, which is expressed as follows:

$$\mathbf{R} = \begin{pmatrix} 1 & \cdots & r_{1N} \\ \vdots & \ddots & \vdots \\ 1/r_{1N} & \cdots & 1 \end{pmatrix} \tag{1}$$

where r represents the scale value representing the relative importance of each indicator, and N denotes the total number of risk assessment indicators.

(3) Consistency verification: The consistency of the judgment matrix is evaluated to adjust the relative importance of indicators until the specified requirements are met.
(4) Weight determination: The judgment matrix is first normalized by columns. Subsequently, the row averages are calculated.

Definition 1. The 5-point scale method assigns values from 1 to 5 to represent the relative importance of indicators, as shown in Table 1.

The risk of human operational errors is highly contingent on expert experience. The consistency check mechanism in AHP ensures the logical coherence of expert judgments. However, uncertainty arises when experts confront novel scenarios, leading to inaccuracies in the assessment results. To address this limitation, qualitative judgments are essential. The 5-point scale approach allows for the formalization of experts' fuzzy judgments, enhancing the generalization capability of the DW-TDFE model and enabling relatively accurate risk assessments even under previously unobserved conditions.

Other weighting methods also exhibit inherent limitations that hinder their suitability for dynamic risk assessment of human operational errors in oil and gas pipeline systems. For instance, BWM (Best-Worst Method) suffers from limited scalability, the entropy weighting method neglects expert knowledge, ANP (Analytic Network Process) involves computational complexity and poor real-time performance, and the fuzzy comprehensive evaluation method is highly sensitive to parameter variation, resulting in low result stability.

2.2. Cloud model

The cloud model facilitates a bidirectional transformation between qualitative concepts and quantitative data converting the uncertainty and fuzziness of risk factors into probabilistic and membership-based analyses. Using historical data and expert judgments, cloud models corresponding to each risk level are constructed. Subsequently, a forward cloud generator produces the membership degree distribution of risk indicators. The reverse cloud algorithm maps measured data onto the cloud map. Ultimately, risk levels are determined, and associated uncertainties are quantified either through the principle of maximum membership degree or a weighted comprehensive calculation. This

Table 1
The 5-point scale method.

Scale value	Meaning
1	Both indicators are equally important
2	One indicator is important than another
3	One indicator is more important than another
4	One indicator is very important than another
5	One indicator is extremely important compared to another

Table 2
Oil and gas pipeline accidents (from 2012 to 2023).

Risk assessment indicators	Frequency/year	Casualty figures/year
Damage by operator	1.1%,0.3%,0.6%,0.5%,0.8%,0.5%,1.1%,1.1%,0.4%,0.3%,0.8%,1.0%	1,0,0,2,0,0,1,0,5,0,0,17
Incorrect equipment operation	0.5%,0.6%,1.1%,0.3%,0.9%,0.5%,0.8%,0.3%,0.3%,0.4%,0.5%,0.3%	1,1,1,0,1,0,1,0,0,0,0,0
Incorrect installation	1.7%,3.1%,2.8%,1.3%,3.0%,2.5%,1.7%,3.5%,2.8%,2.1%,2.9%,2.3%	0,3,0,0,4,1,0,0,0,1,2,6
Incorrect valve position	2.8%,1.6%,3.3%,2.1%,2.4%,2.2%,1.6%,2.3%,2.1%,2.5%,2.7%,1.8%	0,0,0,0,0,2,0,2,0,0,0,0
Other incorrect operation	3.1%,4.7%,3.7%,2.9%,3.8%,5.1%,3.8%,4.6%,3.5%,2.7%,2.2%,2.3%	1,1,6,2,0,0,8,6,0,0,0,0
Overfill of tank	1.6%,1.8%,1.7%,1.4%,1.4%,2.6%,2.1%,2.0%,2.3%,1.6%,1.9%,1.5%	0,0,0,0,0,0,0,0,0,0,0,0
Pipeline overpressured	0.9%,0.8%,1.0%,0.6%,0.8%,0.8%,0.9%,0.8%,1.0%,0.5%,1.1%,0.8%	0,0,0,0,0,0,26,0,0,0,0,0

approach enables a dynamic multi-dimensional risk assessment while preserving data randomness and fuzziness. The calculation flowchart of the cloud model is illustrated in Fig. 1.

2.3. TOPSIS

The TOPSIS provides a robust framework for ranking multi-dimensional risk indicators by evaluating their relative proximity to both positive and negative ideal solutions. First, a risk assessment matrix is established and normalized to eliminate dimensional inconsistencies among the indicators. The weights of each risk indicator are determined using either objective approaches, such as the entropy weight method, or subjective methods based on expert judgment. Next, the Euclidean distances from each assessment object to the positive ideal solution (representing the optimal scenario) and the negative ideal solution (representing the worst-case scenario) are calculated. Finally, the relative closeness of each object to the ideal solution is computed, enabling a ranking of risk levels. This process provides an objective prioritization of high-risk indicators, supporting decision-making in contexts characterized by multi-criteria conflicts. The specific process is illustrated in Fig. 2.

The TOPSIS algorithm is well-suited to risk assessment applications. By calculating the relative closeness of each evaluation indicator to the positive and negative ideal solutions, TOPSIS enables an intuitive quantification and ranking of risk levels. This aligns with the objective of risk assessment—to identify critical risk factors and minimize potential losses—thereby providing a sound basis for managerial decision-making. Moreover, TOPSIS can simultaneously accommodate both quantitative and qualitative information, which is essential for integrating structured accident statistics with fuzzy data derived from human operational errors. Furthermore, the algorithm's linear computational structure facilitates real-time monitoring, making it particularly suitable for dynamic risk assessment scenarios where timeliness is crucial.

2.4. Data enhancement

The time-series data enhancement method based on sliding-window summation incorporates two core operations. First, symmetric padding is applied to both ends of the original sequence to ensure full coverage of boundary data and to prevent information loss at the edges. Second, for each time point, the values of the two preceding and two succeeding observations are aggregated. The original single-point value is replaced by the sum within the sliding window. This procedure enhances the representation of local temporal trends.

Fig. 3 illustrates several representative scenarios for this method:

1. When a single time point exhibits an outlier, sliding-window summation effectively attenuates its impact while preserving the underlying trend (Fig. 3(a)).
2. In cases where isolated observations fail to accurately reflect risk density, the cumulative value within the window captures localized risk aggregation more accurately (Fig. 3(b)).
3. When boundary information is distorted due to incomplete time windows, mirror-symmetric padding preserves edge signals and prevents information loss (Fig. 3(c)).

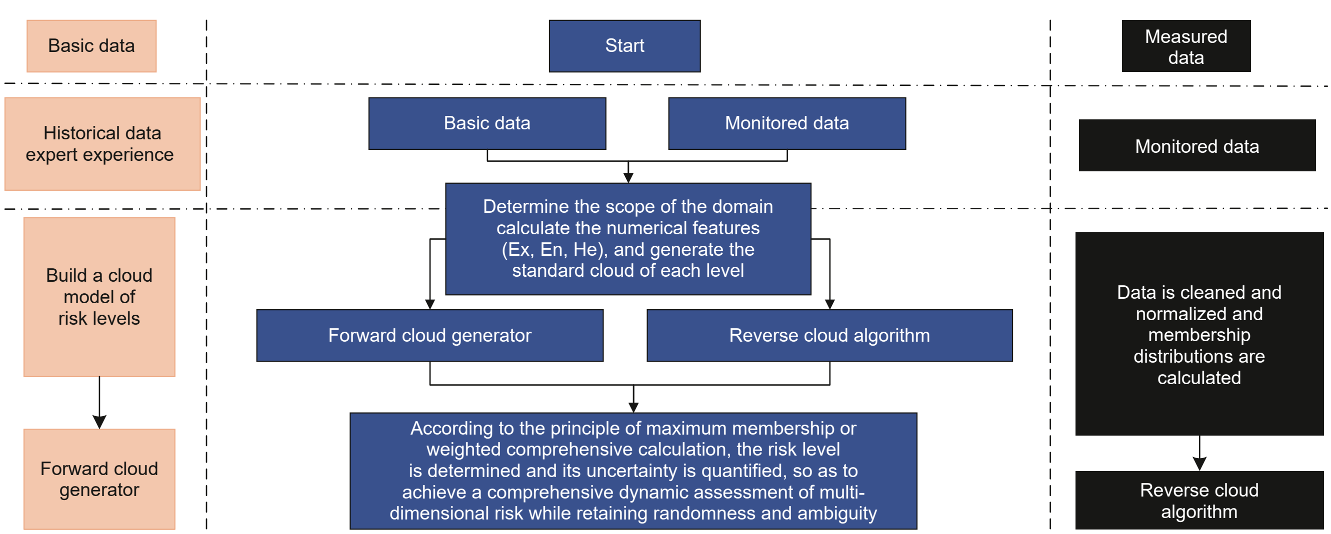

Fig. 1. Flowchart of the cloud model.

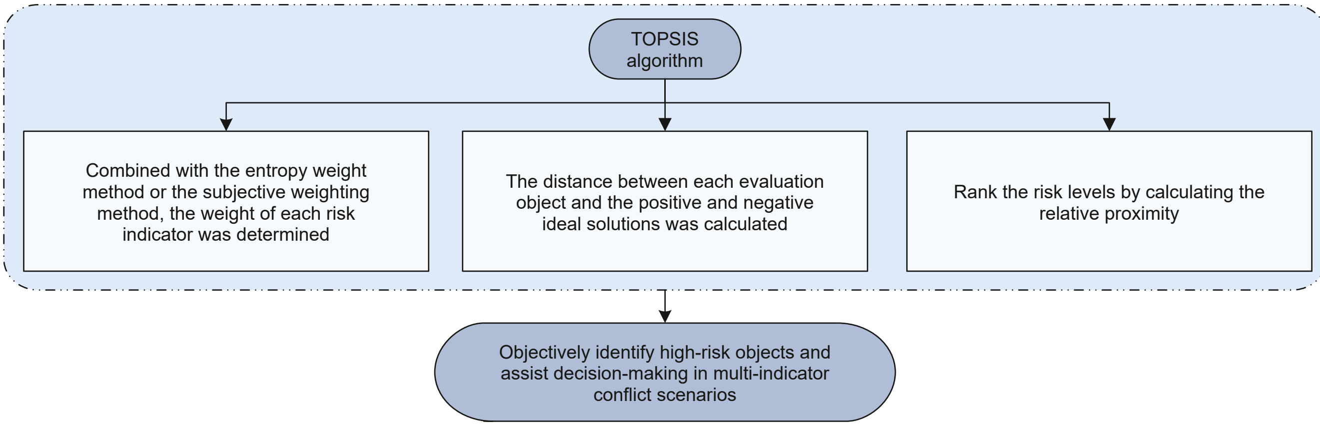

Fig. 2. Flowchart of the TOPSIS algorithm.

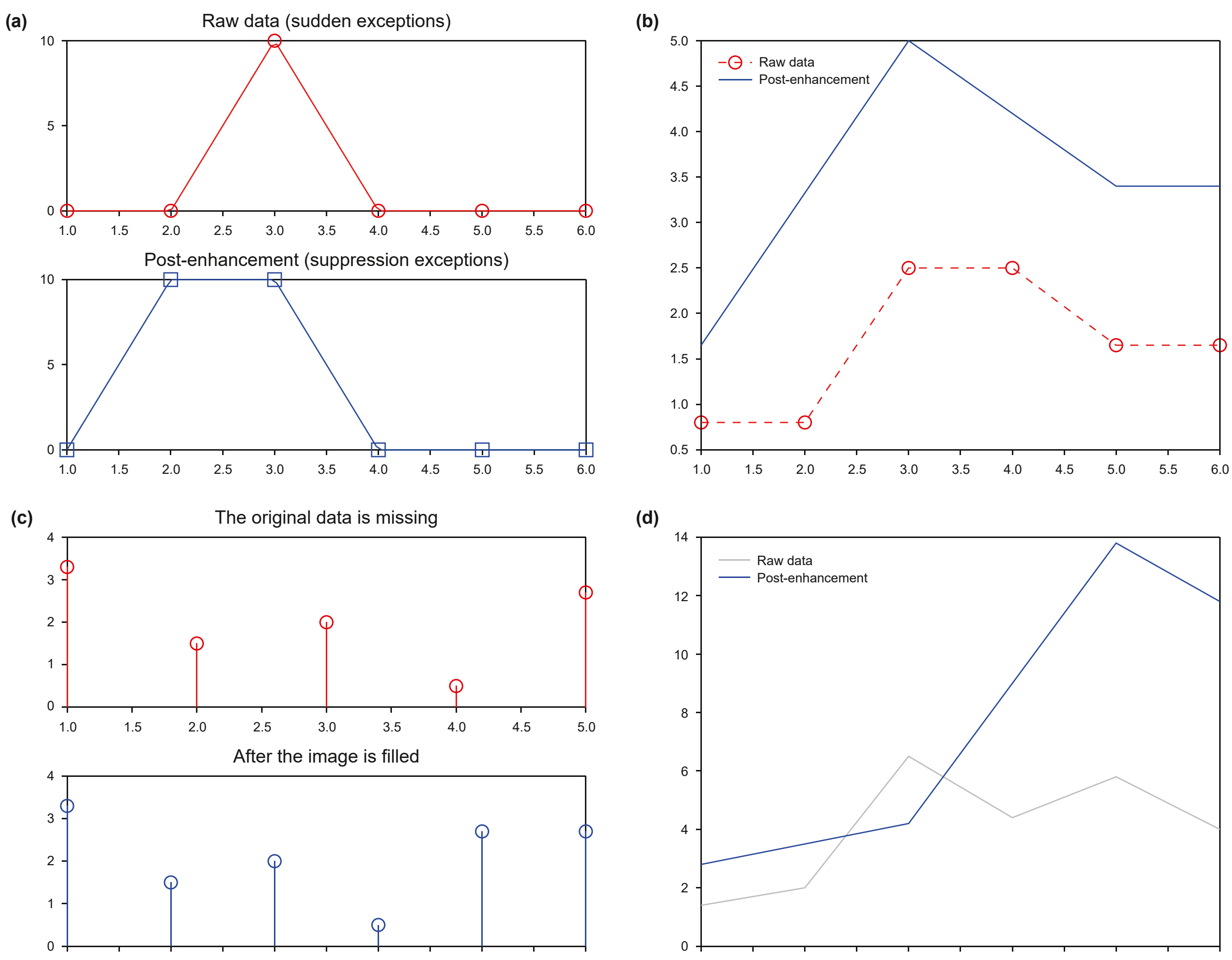

Fig. 3. Representative scenarios for the time-series data enhancement method. **(a)** The single point denotes an outlier. **(b)** Isolated data points fail to accurately reflect risk density. **(c)** The start and end points experience information loss. **(d)** Short-term fluctuations obscure long-term trends.

4. When short-term fluctuations obscure long-term risk dynamics, dynamics, sliding-window summation emphasizes persistent risk signals and smooths transient noise (Fig. 3(d)).

2.5. Performance metrics

Temporal stability (TS) assesses a model's ability to maintain consistent performance. Given that dynamic risk assessment models are typically employed for long-term monitoring and decision-making, ensuring stability across different time intervals is essential. Risk differentiation index (RDI) quantifies the model's capacity to distinguish between indicators of varying severity within the same time segment. This metric is particularly relevant in scenarios with sparse risk occurrences, reflecting the model's ability to detect minority risk classes.

Historical trend fitting evaluates the model's retrospective accuracy in capturing the evolution patterns of risk over time. A high fitting degree ensures that the model reliably reflects past risk dynamics, providing a reliable foundation for accident analysis and informing the design of preventive measures.

The integration of temporal stability and risk differentiation offers a comprehensive evaluation of the model, balancing short-term precision with long-term usability. The calculation formula is as follows:

$$\mathrm{TS} = \max\left(0, \min\left(1, 1\frac{1}{(\tau-1)(\mathrm{RC}_{\max}-\mathrm{RC}_{\min})}\sum_{t}^{\tau-1}\left|\frac{\mathrm{RC}_{t+1}-\mathrm{RC}_{t}}{T_{t+1}-T_{t}}\right|\right)\right) \tag{2}$$

where τ represents the total number of time segments, t is the current segment, RC denotes the comprehensive closeness degree of risk assessment indicators, and T is the full time horizon.

Based on membership degrees, each risk indicator is classified into either the high membership degree set μ_{high} or the low membership degree set μ_{low}:

$$\begin{cases} \mu_{\mathrm{high}}\, f\cdot\sqrt{c} > 0, \mu > 0.5 \\ \mu_{\mathrm{low}} f\cdot\sqrt{c} < 0, \mu < 0.5 \end{cases} \tag{3}$$

where μ_{high} is the high membership degree set, μ_{low} represents the low membership degree set, f denotes the frequency of risk evaluation indicators, c is the number of casualties, and μ signifies the membership degree.

The mean membership degrees for each set are computed as:

$$\mathrm{mean}_{\mathrm{high}} = \frac{1}{\tau}\sum_{t=1}^{\tau}\mu_{\mathrm{high}} \tag{4}$$

$$\mathrm{mean}_{\mathrm{low}} = \frac{1}{\tau}\sum_{t=1}^{\tau}\mu_{\mathrm{low}} \tag{5}$$

where $\mathrm{mean}_{\mathrm{high}}$ and $\mathrm{mean}_{\mathrm{low}}$ represent the mean membership degrees for the high and low membership degree sets, respectively.

The standard deviations of the membership degrees for both sets are calculated as:

$$\sigma_{\mathrm{high}} = \sqrt{\frac{1}{\tau-1}\sum_{t=1}^{\tau}\left(\mu_{\mathrm{high}} - \mathrm{mean}_{\mathrm{high}}\right)} \tag{6}$$

$$\sigma_{\mathrm{low}} = \sqrt{\frac{1}{\tau-1}\sum_{t=1}^{\tau}\left(\mu_{\mathrm{low}} - \mathrm{mean}_{\mathrm{low}}\right)} \tag{7}$$

where σ_{high} and σ_{low} denote the standard deviations of the membership degrees for the high and low membership degree sets, respectively.

$$\mathrm{RDI} = \frac{\mathrm{mean}_{\mathrm{high}} - \mathrm{mean}_{\mathrm{low}}}{\sigma_{\mathrm{high}} - \sigma_{\mathrm{low}}} \tag{8}$$

The historical trend fitting degree is calculated as:

$$\mathrm{RDI} = 1 - \frac{1}{T}\sum_{t=1}^{T}\frac{|\mathrm{output\ model}(t) - \mathrm{output}_{\mathrm{actual}}(t)|}{n_{\mathrm{risk\ level}} - 1} \tag{9}$$

where HTF represents the historical trend fitting degree, T denotes the total number of time segments, $\mathrm{output}_{\mathrm{model}}$ is the model output, $\mathrm{output}_{\mathrm{actual}}$ represents the observed outcome, and $n_{\mathrm{risk\_level}}$ signifies the number of risk levels.

2.6. Summary

AHP is employed to compute the initial weights of risk assessment indicators, which are then used to derive dynamic weights. By introducing Gaussian noise and a time decay factor, the model simulates real-world disturbances and regulates the amplitude of weight fluctuations. This dynamic adjustment mechanism is further refined via entropy regulation and a hyperbolic tangent function. This ensures that the computed weights remain aligned with expert judgment while enhancing responsiveness to real-time changes, thus improving both accuracy and robustness. To address fragmentation and noise in the original data, time-series data enhancement techniques—such as mirror padding and sliding window summation—are applied to generate smooth sequences, providing high-quality input for dynamic membership functions. These functions are trained using a gradient descent algorithm that maximizes the log-likelihood function, iteratively optimizing shape parameters and risk thresholds. Consequently, the dynamic membership functions more accurately map risk levels, enabling the construction of a three-dimensional fuzzy matrix heatmap that captures the temporal evolution of risk across assessment indicators. The integration of cloud models converts dynamic weights and enhanced data into cloud parameters (including expectation, entropy, and hyper-entropy), which quantify the uncertainty and ambiguity inherent in human operational errors. The improved TOPSIS algorithm combines these cloud parameters with dynamic weights through weighted cloud distances, calculating the relative distances of each indicator to positive and negative ideal solutions. A standard deviation correction term further strengthens adaptability to temporal fluctuations, yielding a comprehensive closeness measure. This enables effective prioritization of risk assessment indicators, and enhances the model's ability to capture evolving risk trends.

3. Construction of the DW-TDFE model

3.1. Risk assessment indicator system architecture

Based on data obtained from the PHMSA website, a two-tiered risk assessment indicator system was constructed. The first tier encompasses human operational error as the primary risk domain. The second tier includes seven specific sub-indicators: damage by operators, incorrect equipment operation, incorrect installation, incorrect valve position, other incorrect operation, overfill of tank, and pipeline overpressured.

3.2. Algorithmic process

The DW-TDFE model is built upon dynamic weights and a three-dimensional fuzzy matrix. It integrates a data-driven dynamic membership function with enhanced data processing to improve temporal stability, risk discrimination, and overall assessment accuracy. The workflow of the DW-TDFE model is illustrated in Fig. 4.

The algorithmic process involves three core steps:

Step 1: Dynamic weight determination.

To achieve adaptive equilibrium in the risk assessment weight system, a dynamic weight calculation algorithm is designed based on entropy regulation and time decay principles. To enhance sensitivity to abrupt changes in risk data, Gaussian noise is introduced to simulate real-world fluctuations. The uncertainty associated with each indicator is quantified through entropy values. The time decay mechanism ensures a smooth temporal update of weights, preventing abrupt fluctuations and allowing the model to emphasize long-term risk trends rather than being disproportionately influenced by short-term anomalies. To further improve temporal stability, a hyperbolic tangent function is employed to compress the amplitude of weight fluctuations. Finally, the dynamic weights are normalized to maintain a balanced distribution across all indicators and time periods.

Log-normal weights preserving the characteristics of the initial weights $\omega_{\text{AHP}}^{(i)}$ are generated using:

$$\omega_{\text{AHP}}^{(i)} = \omega_{\text{initial}} \odot \exp(\varepsilon_{\text{GN}}),\ \varepsilon_{\text{GN}} \sim \text{N}\left(0, \sigma^2\right) \tag{10}$$

$$\sigma = \max\left(\frac{\text{std}(\omega_{\text{initial}})}{\text{mean}(\omega_{\text{initial}})}\right) \times \beta \tag{11}$$

where i represents the risk assessment indicator; σ is the standard deviation of historical weight data; β denotes the noise expansion factor, determined through sensitivity analysis (Section 4.2). This factor ensures that the noise intensity slightly exceeds observed fluctuations to adequately capture real-world uncertainty; $\odot$ signifies element-wise multiplication; ε_{GN} is the Gaussian noise, simulating disturbances due to environmental interference, data collection errors, and other uncertainties. The zero-mean ensures symmetric perturbations around the initial weights, thereby avoiding systematic bias. Gaussian noise is transformed into a log-normal distribution through $\exp(\varepsilon_{\text{GN}})$ enforce $\omega_{\text{AHP}}^{(i)} > 0$.

The composite entropy parameter He_ω is calculated as follows:

$$\text{En}_\omega = \text{std}\left(\omega_{\text{AHP}}^{(i)}\right) \tag{12}$$

$$\text{He}_{\min} = \text{quantile}\left(\text{En}_\omega, \text{Q}_{\text{En}_\omega}\right) \tag{13}$$

$$\text{He}_\omega = \text{En}_\omega \cdot \text{e}^{-t/\tau} + \text{He}_{\min} \tag{14}$$

where En_ω is the standard deviation of weights for each indicator. $\text{Q}_{\text{En}_\omega}$ represents the minimum quantile threshold for entropy, derived from the historical distribution of weight standard deviations to prevent excessively low uncertainty from causing weight adjustment failures; quantile represents the linear interpolation function; $\text{e}^{-t/\tau}$ is the time decay factor, controlling the influence of historical data on current weights; τ represents the time decay period, set according to the assessment cycle. This ensures that more recent data are assigned greater importance.

The dynamic weight adjustment function (adjustment_matrix) is defined as:

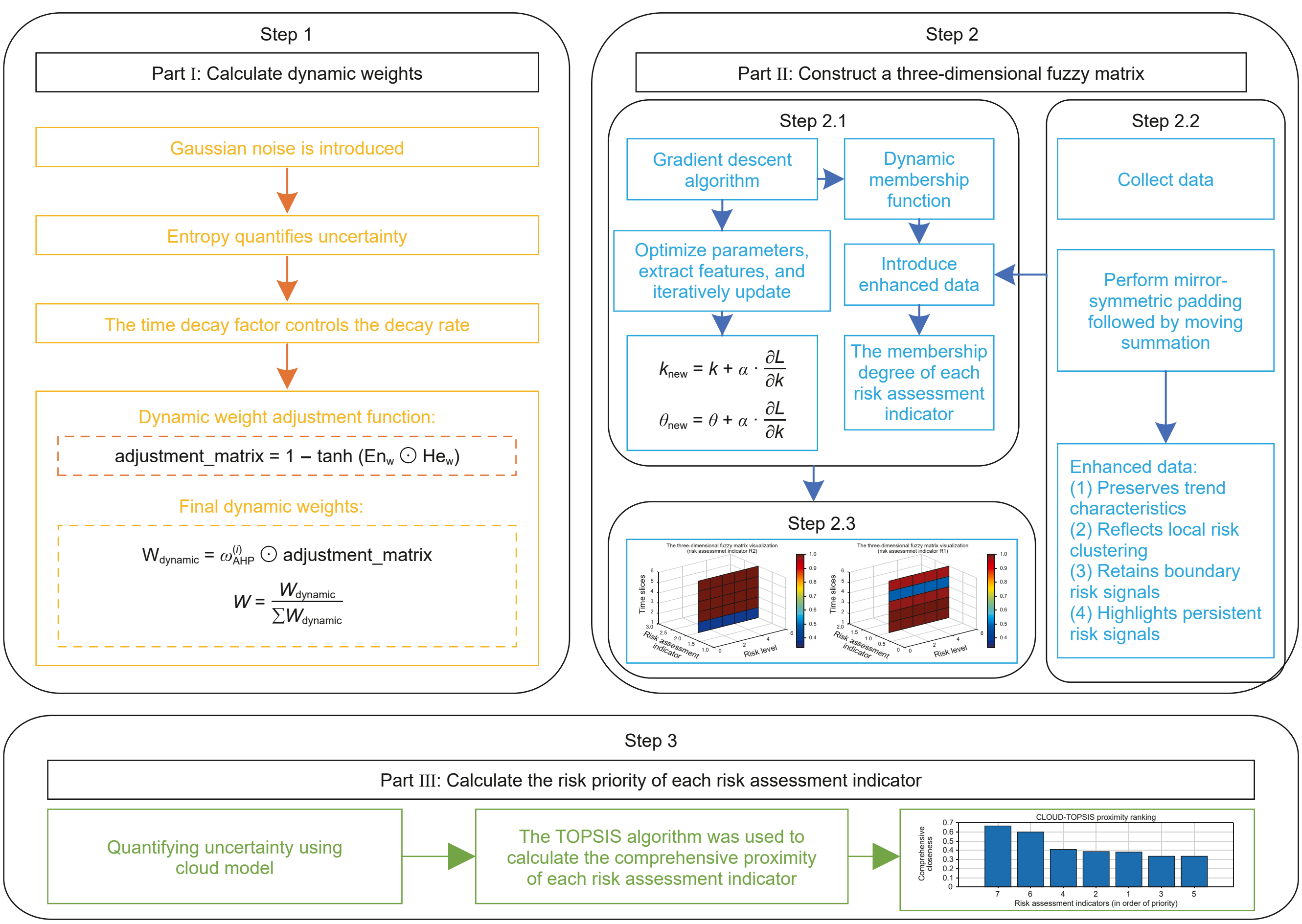

Fig. 4. The DW-TDFE model.

$$\text{adjustment\_matrix} = 1 - \tanh(\text{En}_\omega \odot \text{He}_\omega) \tag{15}$$

where tanh represents the hyperbolic tangent function.

The final dynamic weight W is computed as:

$$W_{\text{dynamic}} = \omega_{\text{AHP}}^{(i)} \odot \text{adjustment\_matrix} \tag{16}$$

$$W = \frac{W_{\text{dynamic}}}{\sum W_{\text{dynamic}}} \tag{17}$$

where W_{dynamic} represents the unnormalized dynamic weight.

The entropy-based dynamic weight adjustment relies on two key parameters: the entropy parameter En_ω and the hyper-entropy parameter He_ω. The entropy parameter quantifies the uncertainty of each risk assessment indicator, derived from the standard deviation of its historical weight series. The hyper-entropy parameter comprises the time decay factor $e^{-t/\tau}$ and the minimum quantile threshold Q_{En_ω}. The threshold prevents the hyper-entropy parameter from decaying to zero, thus maintaining long-term stability. The time decay factor $e^{-t/\tau}$ is computed based on the current time point t and the time decay period τ, which varies with the interval between consecutive assessment points.

Step 2: Construction of the three-dimensional fuzzy matrix.

Step 2.1: To accurately map risk levels, the parameters of the dynamic membership functions are optimized using the gradient descent algorithm (Fu et al., 2025). Considering the distributional characteristics of accident frequency and casualty data, the optimization objective is formulated based on the maximum likelihood estimation principle. During iterative optimization, the algorithm yields optimal parameters and corresponding risk membership degrees. The shape parameter k is set to 1, representing a standard reference function; the risk threshold θ is also set to 1, consistent with the risk level quantification rules defined below; the convergence threshold ε is set to 10^{-6}, ensuring that the final membership values attain a precision level of 10^{-4}, which satisfies the accuracy requirements for risk assessment. The selection of the maximum number of iterations and the learning rate is illustrated in Fig. 5.

As shown in Fig. 5, the left panel depicts the influence of the learning rate α on the convergence speed of the gradient descent algorithm. The x-axis represents the learning rate α, and the y-axis denotes the number of iterations required for convergence, with larger values indicating slower convergence. The blue curve connects the number of iterations corresponding to each learning rate, reflecting the overall trend. Green circles indicate learning rates at which convergence is achieved, whereas red circles represent learning rates that fail to converge. The right panel demonstrates the effect of the learning rate α on the model's fitting performance. The x-axis denotes the learning rate, while the y-axis represents the final log-likelihood value, with higher values indicating better alignment between the model and observed data. The blue curve links the final log-likelihood values for various learning rates, illustrating the relationship between learning rate variations and model fitting. Within an effective range, the learning rate α has minimal impact on model fitting. Green and red filled circles mark converged and non-converged learning rates, respectively. The effective learning rate intervals for each risk assessment indicator are identified as: [0.01,0.2], [0.01,0.2], [0.001,0.2], [0.01,0.2], [0.001, 0.02], [0.01, 0.2], and [0.005, 0.2]. In most cases, setting $\alpha = 0.01$ achieves a relatively higher final log-likelihood, indicating optimal model fit. Similarly, a maximum number of iterations of 1000 ensures convergence in the majority of risk assessment scenarios, balancing computational efficiency with robustness against marginal data variations.

The dynamic membership function μ_{dynaminc} is defined as:

$$\mu_{\text{dynamic}} = \frac{1}{1 + e^{-k\cdot(f\cdot\sqrt{c} - \theta)}} \tag{18}$$

where k is the shape parameter, controlling the sensitivity of the dynamic membership function, and θ represents the risk threshold. Both parameters are optimized via the gradient descent algorithm, with the maximum likelihood function as the objective.

The maximum log-likelihood optimization objective function L is given by:

$$L = \sum_{i=1}^{N} \left[y_i \cdot \ln\left(\mu_{\text{dynamic}}^i\right) + (1 - y_i) \cdot \ln\left(1 - \mu_{\text{dynamic}}^i\right) \right] \tag{19}$$

where y_i denotes the risk level of each risk assessment indicator.

The partial derivatives of L with respect to k and θ are computed using the chain rule:

$$\frac{\partial L}{\partial k} = \sum_{i=1}^{N} \left(y_i - \mu_{\text{dynamic}}^i\right) \cdot (f_i \cdot \sqrt{c_i} - \theta) \tag{20}$$

$$\frac{\partial L}{\partial \theta} = \sum_{i=1}^{N} \left(\mu_{\text{dynamic}}^i - y_i\right) \cdot k \tag{21}$$

Parameters are iteratively updated according to:

$$k_{\text{new}} = k + \alpha \cdot \frac{\partial L}{\partial k} \tag{22}$$

$$\theta_{\text{new}} = \theta + \alpha \cdot \frac{\partial L}{\partial \theta} \tag{23}$$

where α is the learning rate, and k_{new} and θ_{new} are the updated values.

The termination condition is defined as:

$$\left| L_{\text{current}} - L_{\text{prev}} \right| < \varepsilon \tag{24}$$

where ε is the convergence threshold, L_{current} denotes the log-likelihood value in the current iteration, and L_{prev} is the log-likelihood value in the previous iteration.

Step 2.2: Mirror-symmetric padding is applied to the boundaries of the dataset. Subsequently, a moving summation is conducted within a predefined temporal window over the occurrence frequency of risk indicators and the number of casualties, generating an enhanced data matrix consisting of cumulative values. This approach reduces short-term fluctuations while capturing mid-to long-term evolution patterns through window-based accumulation. The procedure involves the following steps:

Data normalization:

$$f_1 = \frac{f}{\sum_{i=1}^{n} f_i} \tag{25}$$

$$c_1 = \begin{cases} \dfrac{c}{\sum_{i=1}^{n} c_i} & \text{not all values of } c \text{ are zero} \\ 0 & \text{all values of } c \text{ are zero} \end{cases} \tag{26}$$

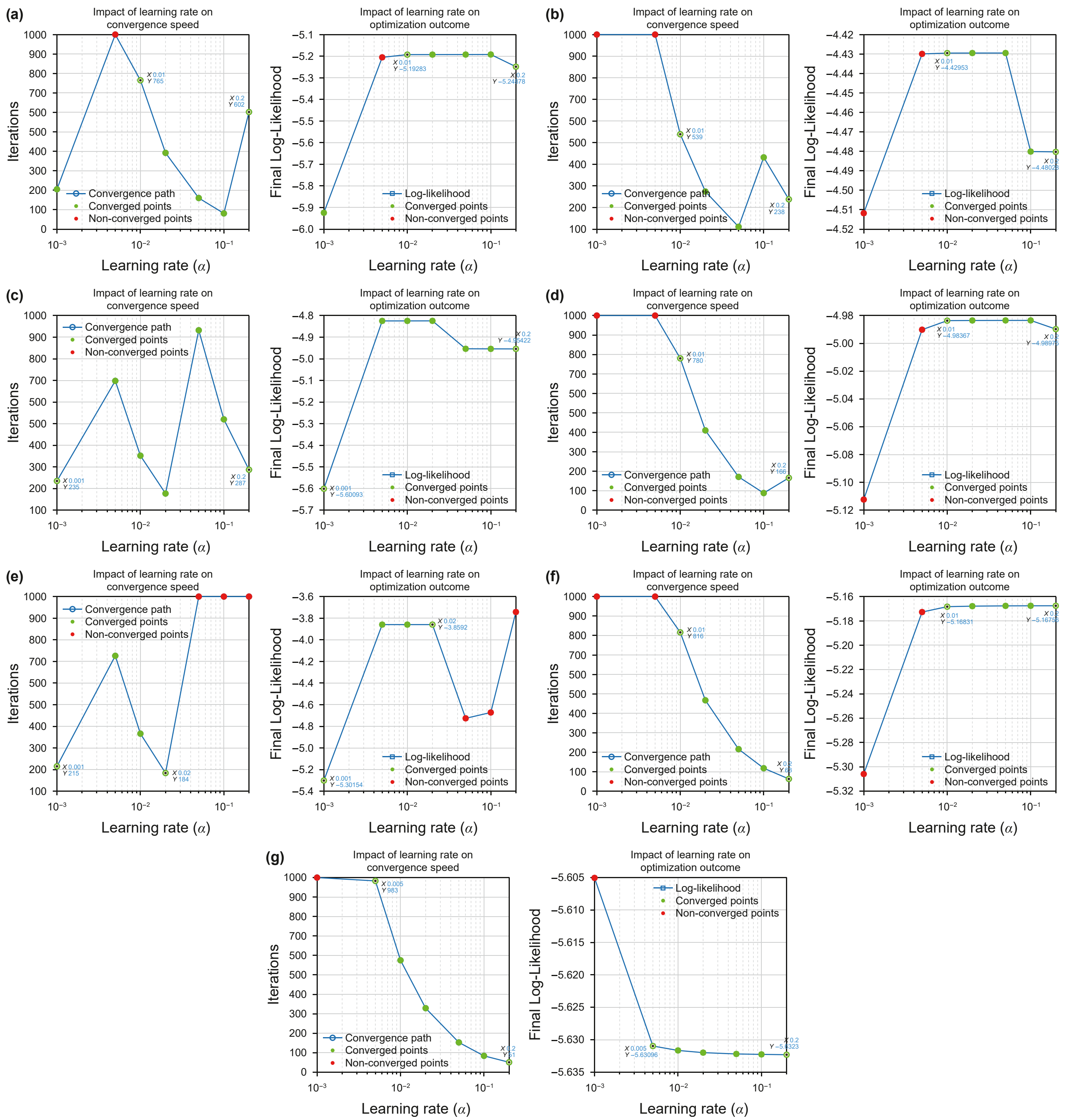

Fig. 5. The training process of the gradient descent algorithm. **(a)** Damage by operator, **(b)** incorrect equipment operation, **(c)** incorrect installation, **(d)** incorrect valve position, **(e)** other incorrect operation, **(f)** overfill of tank, **(g)** pipeline overpressured.

Mirror padding:

$$\text{padded\_f}=\left[f_1(1),\cdots,f_1\left(p_{\text{left}}\right),f_1(1),\cdots,f_1(N),f_1\left(i\text{–}p_{\text{right}}+1\right),\cdots,f_1(N)\right] \tag{27}$$

$$\text{padded\_c}=\left[c_1(1),\cdots,c_1\left(p_{\text{left}}\right),c_1(1),\cdots,c_1(N),c_1\left(i\text{–}p_{\text{right}}+1\right),\cdots,c_1(N)\right] \tag{28}$$

where padded_f and padded_c represent the occurrence frequency and casualty count, respectively.

The padding length on both sides of each time series is computed as:

$$p_{\text{left}}=\left\lfloor\frac{\text{window\_size–1}}{2}\right\rfloor \tag{29}$$

$$p_{\text{right}}=\left\lceil\frac{\text{window\_size–1}}{2}\right\rceil \tag{30}$$

where window_size denotes the time-span parameter, determined by the assessment window. It controls the range of local smoothing.

Enhanced data:

$$\text{enhancement\_data}(f) = \sum_{m=t}^{t+\text{window\_size}-1} \text{padded\_}f(m) \quad (31)$$

$$\text{enhancement\_data}(c) = \sum_{m=t}^{t+\text{window\_size}-1} \text{padded\_}c(m) \quad (32)$$

Step 2.3: A three-dimensional fuzzy matrix is constructed to characterize the dynamic relationships between risk indicators, risk levels, and time periods. This matrix is derived from the enhanced datasets of event frequency and casualty counts. A dynamic membership function is employed to determine the distribution of membership degrees for each risk indicator across risk levels within each time period.

Step 3: The cloud model is integrated with the improved TOPSIS algorithm to obtain weighted cloud distances for each time period. Risk uncertainty is quantified via the expectation, entropy, and hyper-entropy of positive and negative ideal solutions. Finally, the comprehensive closeness of each risk indicator to the ideal solutions is computed, which is then used to rank the risk indicators.

The weighted cloud distance d_i is calculated as follows:

$$d_i = \sqrt{\sum_{j=1}^{n} W_t^{(i)} \left[\left(\text{Ex}_j - R_{ij} \right)^2 + \text{En}_j^2 + \text{He}_j^2 \right]} \quad (33)$$

where $W_t^{(i)}$ denotes the dynamic weight of the i-th risk indicator in the t-th time period; Ex_j, En_j, He_j represent the expectation, entropy, and hyper-entropy of the cloud model, respectively; R_{ij} is the membership degree of the i-th risk indicator at the j-th risk level.

The cloud parameters (Ex_j, En_j, He_j) are calculated as:

$$\begin{cases} \text{Ex}_j = \max\left(R_{\cdot j}\right) \text{ positive ideal solution} \\ \text{Ex}_j = \min\left(R_{\cdot j}\right) \text{ negative ideal solution} \end{cases} \quad (34)$$

$$\text{En}_j = \text{std}\left(R_{\cdot j}\right) \quad (35)$$

$$\text{He}_j = \text{En}_j \cdot e^{-t/\tau} \quad (36)$$

The improved comprehensive closeness RC is defined as:

$$\sigma^+ = \text{std}(R_t \odot W_t) \quad (37)$$

$$\sigma^- = \text{std}(R_t \odot (1 - W_t)) \quad (38)$$

$$\text{RC} = 1 - \frac{d^- + \sigma^-}{d^+ + d^- + \sigma^+ + \sigma^-} \quad (39)$$

where σ^+ denotes the standard deviation of the product of weights and membership degrees across all risk indicators; σ^- represents the standard deviation of the product of complementary weights and membership degrees; d^+ and d^- are the distances to the positive and negative ideal solutions, respectively.

The improved TOPSIS algorithm incorporates the dynamic weight $W_t^{(i)}$ into the weighted cloud distance calculation, enabling the model to adapt to time-varying risk profiles. To further strengthen temporal sensitivity, a time decay factor is introduced to assign greater importance to more recent observations. This weighting strategy ensures that current risk conditions are emphasized while diminishing the influence of outdated information, thereby improving both tracking accuracy and temporal robustness. Moreover, a standard deviation correction term is incorporated into the comprehensive closeness formulation to account for the volatility of weights and membership degrees. This correction allows the model to adjust closeness values in response to data volatility, thus reducing misjudgments and enhancing robustness against outliers.

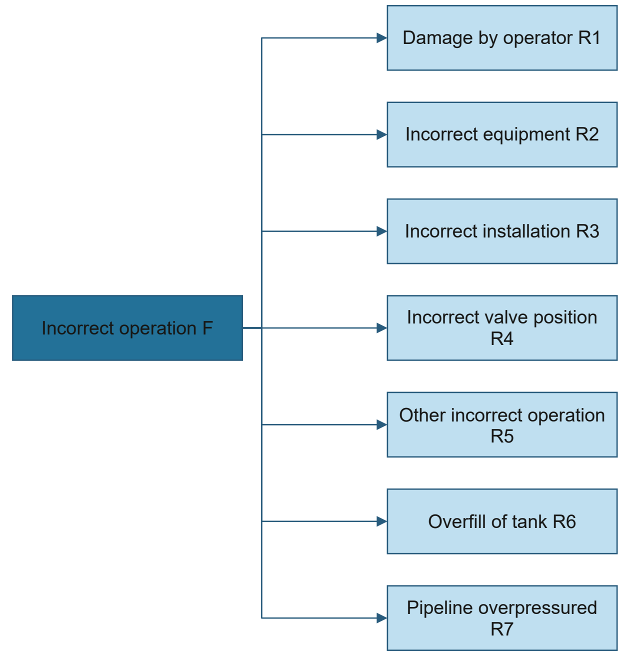

Fig. 6. Risk indicator system.

The improved TOPSIS algorithm effectively addresses several limitations of the traditional approach. To overcome the inability of fixed weights to accommodate dynamic risk assessment, entropy-based adjustment and time-decay factors are introduced to construct dynamic weighting schemes. To manage the fuzziness and randomness intrinsic to risk data, the improved TOPSIS algorithm is integrated with the cloud model, which transforms enhanced data and dynamic weights into cloud parameters, enabling a quantitative representation of uncertainty under fuzzy conditions. Furthermore, to suppress noise interference that compromises the stability of traditional TOPSIS results, a standard deviation correction term is incorporated into the calculation of the comprehensive closeness degree. This reduces the influence of short-term fluctuations on long-term trends, thereby enhancing model robustness. The improved TOPSIS algorithm functions as an integrator in the DW-TDFE model. It receives dynamic cloud weights and three-dimensional fuzzy matrix outputs and utilizes the results of data augmentation and fuzzy processing to compute comprehensive closeness coefficients. This supports risk classification and heat map generation, fulfilling the analysis of three-dimensional risk evolution.

According to Eq. (39), a higher closeness corresponds to a greater distance from the negative ideal solution, indicating a lower risk priority for the associated risk indicator.

Table 3
Weights of the second-level risk assessment indicators.

Time period	Weights						
First	0.0659	0.0621	0.2753	0.1222	0.2974	0.1106	0.0665
Second	0.2572	0.0381	0.1079	0.1703	0.1699	0.1157	0.0407
Third	0.1451	0.1442	0.1857	0.2035	0.2361	0.0828	0.0026
Fourth	0.0519	0.1937	0.1454	0.2072	0.2438	0.1048	0.0532
Fifth	0.0543	0.1551	0.2020	0.1686	0.2695	0.0949	0.0556
Sixth	0.1449	0.1430	0.2449	0.0958	0.2617	0.0897	0.0200

4. Case study

According to the PHMSA database, casualties resulting from pipeline overpressure peaked in 2018. This surge can be attributed to the large-scale upgrading of supervisory control and data acquisition systems undertaken by relevant enterprises during that period. Due to insufficient familiarity with the newly deployed systems, operators were unable to promptly detect and appropriately respond to abnormal monitoring data. In subsequent years, the proportion of accidents attributed to human operational errors remained at approximately 10%, with an average of around ten casualties reported annually. Human error has consistently ranked among the two most critical risk factors affecting the safety of oil and gas pipelines. Therefore, conducting risk assessments targeting human operational error is crucial.

This paper proposes a DW-TDFE model for evaluating human operational errors in oil and gas pipelines. To evaluate the performance of the DW-TDFE model, an empirical analysis was conducted using accident data from 2012 to 2023 obtained from the PHMSA database. These data were utilized to identify relevant risk indicators, establishing a risk indicator system. The process comprises five stages: text mining, network construction, topological analysis, mechanism supplementation, and indicator system generation. This framework supports the development of a hybrid-driven risk evaluation model, thereby enhancing data-driven risk management capabilities (Lu et al., 2025a). The model can be extended to AI-driven risk assessment, enabling an integrated risk management process of "identification-assessment-control" (Lu et al., 2025b). The collected accident records were filtered using the keyword "incorrect operation". Human operational error was designated as the first-level indicator, while damage by operator, incorrect equipment operation, incorrect installation, incorrect valve position, other incorrect operation, overfill of tank, and pipeline overpressured were classified as second-level indicators. The risk indicator system is illustrated in Fig. 6.

4.1. Example description

(1) The data collected from the PHMSA website are presented in Table 2.

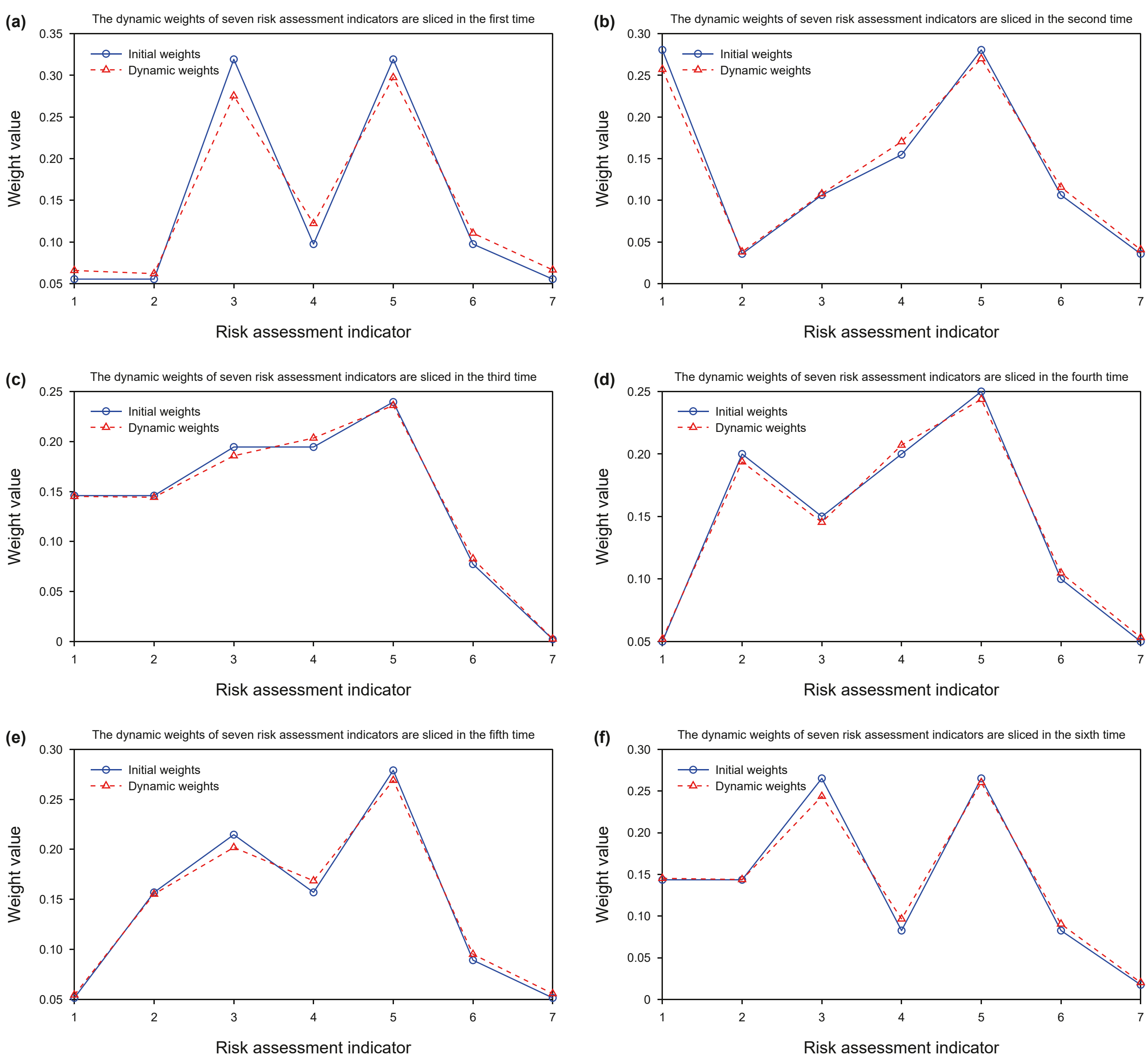

Fig. 7. The temporal trend of weights. **(a)** The first time period. **(b)** The second time period. **(c)** The third time period. **(d)** The fourth time period. **(e)** The fifth time period. **(f)** The sixth time period.

As shown in the second row of Table 2, the frequency of damage by operator from 2012 to 2023 is 1.1%, 0.3%, 0.6%, 0.5%, 0.8%, 0.5%, 1.1%, 1.1%, 0.4%, 0.3%, 0.8%, and 1.0%, respectively. The corresponding number of casualties reported during this period is 1, 0, 0, 2, 0, 0, 1, 0, 5, 0, 0, and 17, respectively. The remaining figures can be derived following the same procedure.

(2) Weight calculation

Each two-year interval was defined as an independent time period for dynamic risk evaluation. First, AHP was employed to determine the initial weights of the second-level indicators. These weights were then incorporated into the dynamic weight calculation algorithm. The results are presented in Table 3, and the temporal trend of these weights is illustrated in Fig. 7.

As shown in Fig. 7, indicators exhibiting greater standard deviations (such as “incorrect installation” and “other incorrect operation” in Fig. 7(a)) experience a substantial reduction in the assigned weights. Conversely, more stable indicators (such as “damage by operator” and “incorrect equipment operation” in Fig. 7(a)) have increased weights.

(3) Construction of the three-dimensional fuzzy matrix

Using the LEC assessment method (Graham and Kinney, 1980), each indicator is classified into six risk levels based on the frequency of occurrence and the number of casualties. These levels are assigned values of 0, 0.2, 0.4, 0.6, 0.8, and 1, with higher values indicating greater risk severity. The classification criteria are detailed in Tables 4 and 5, which were developed in strict accordance with the ISO31000 standard (Lu, 2018).

The final risk level is determined by aggregating the quantified values based on the frequency of occurrence and the number of casualties. To ensure normalization, any composite value exceeding 1 is truncated to 1. Subsequently, the parameters of the dynamic membership function are optimized using the gradient descent algorithm. The results are presented in Table 6. This process takes into account the occurrence frequency, casualty counts, and risk levels across time periods.

The optimal values of k range from 0.0117 (overfilling of the tank) to 2.5190 (other incorrect operation), while the optimal values of θ are between -2.41 (other incorrect operation) and 0.84 (pipeline overpressured), indicating substantial heterogeneity across indicators. Notably, the relatively low θ value for other incorrect operation (-2.4105) suggests a lower risk classification threshold. Therefore, this indicator is classified as high-risk. In contrast, the identical k and θ values for overfill of tank and pipeline overpressured indicate their comparatively weaker impact on the overall risk assessment. This aligns with the prioritization results in Fig. 11, where other incorrect operation exhibits the highest risk priority, and overfill of the tank and pipeline overpressured rank among the lowest. These results demonstrate that the proposed optimization framework can effectively identify optimal values of k and θ. The derived parameters can capture the dynamic responses of the indicators and reflect their relative contributions to the integrated model.

Table 4
Risk level quantification based on the frequency of occurrence.

Frequency	Values
0–0.3%	0
0.3%–0.8%	0.2
0.8%–1.5%	0.4
1.5%–2.5%	0.6
2.5%–4.0%	0.8
>4.0%	1

Table 5
Risk level quantification based on the number of casualties.

Casualty	Values
0	0
1–2	0.2
3–5	0.6
6–8	1

Table 6
Optimization of the dynamic membership function parameters.

Risk assessment indicator	Optimal value of k	Optimal value of θ
Damage by operator	0.2481	0.1405
Incorrect equipment operation	0.6583	0.6583
Incorrect installation	1.3806	-1.1467
Incorrect valve position	0.9355	-0.8923
Other incorrect operation	2.5190	-2.4105
Overfill of tank	0.0117	0.0117
Pipeline overpressured	0.8363	0.8363

Mirror-symmetric padding is applied to the data boundaries, followed by a moving summation of occurrence frequency and casualty counts. This process generates enhanced data incorporating local temporal aggregation effects, as illustrated in Fig. 8.

After enhancing the consequence data for damage by operators, the isolated peak observed in the second time period is redistributed to adjacent periods. This results in a reduction in peak amplitude (Fig. 8(a)). Enhancement of the consequence data for incorrect equipment operation aggregates information across neighboring time periods, effectively suppressing short-term fluctuations (Fig. 8(b)). In Fig. 8(c), enhancing the consequence data for incorrect installation mitigates spikes caused by abrupt increases, broadens transient peaks, reduces volatility, and reinforces periodic features, thereby improving trend coherence. As shown in Fig. 8(d), the enhancement of the consequence data for incorrect valve position results in peak accumulation, indicating the clustering of local risks. Fig. 8(e) depicts that, following data enhancement for other incorrect operations, the trend becomes smoother, with a more distinct long-term directional tendency. In Fig. 8(f) and (g), the consequence data for overfill of tank and pipeline overpressured remain at zero throughout the observation period. For consistency, mirror filling is applied to prevent trend distortion caused by window truncation. With respect to frequency data enhancement, the occurrence rates of all indicators remain relatively low. To mitigate the underestimation of trend variability at the beginning and end of the time series, boundary padding and mirror padding are employed, thus enhancing data continuity and reinforcing long-term cyclical patterns.

Data enhancement primarily aims to suppress short-term volatility and amplify long-term trends. The variance reflects data dispersion, with higher values denoting greater volatility. The model stability before and after data enhancement was examined, along with risk differentiation capability and weight variance reduction rates. The results are shown in Tables 7 and 8.

Data enhancement increased the temporal stability from 0.7726 to 0.7983, and the risk differentiation from 2.65 to 3.09 (Table 7). For damage by operator, the variance reduction rates for the frequency and casualty figures reached 56.90% and 60.84%, respectively (Table 8). This indicates a substantial decline in data volatility, thereby confirming the efficiency of the sliding window. The model exhibited a marked reduction in noise sensitivity (as

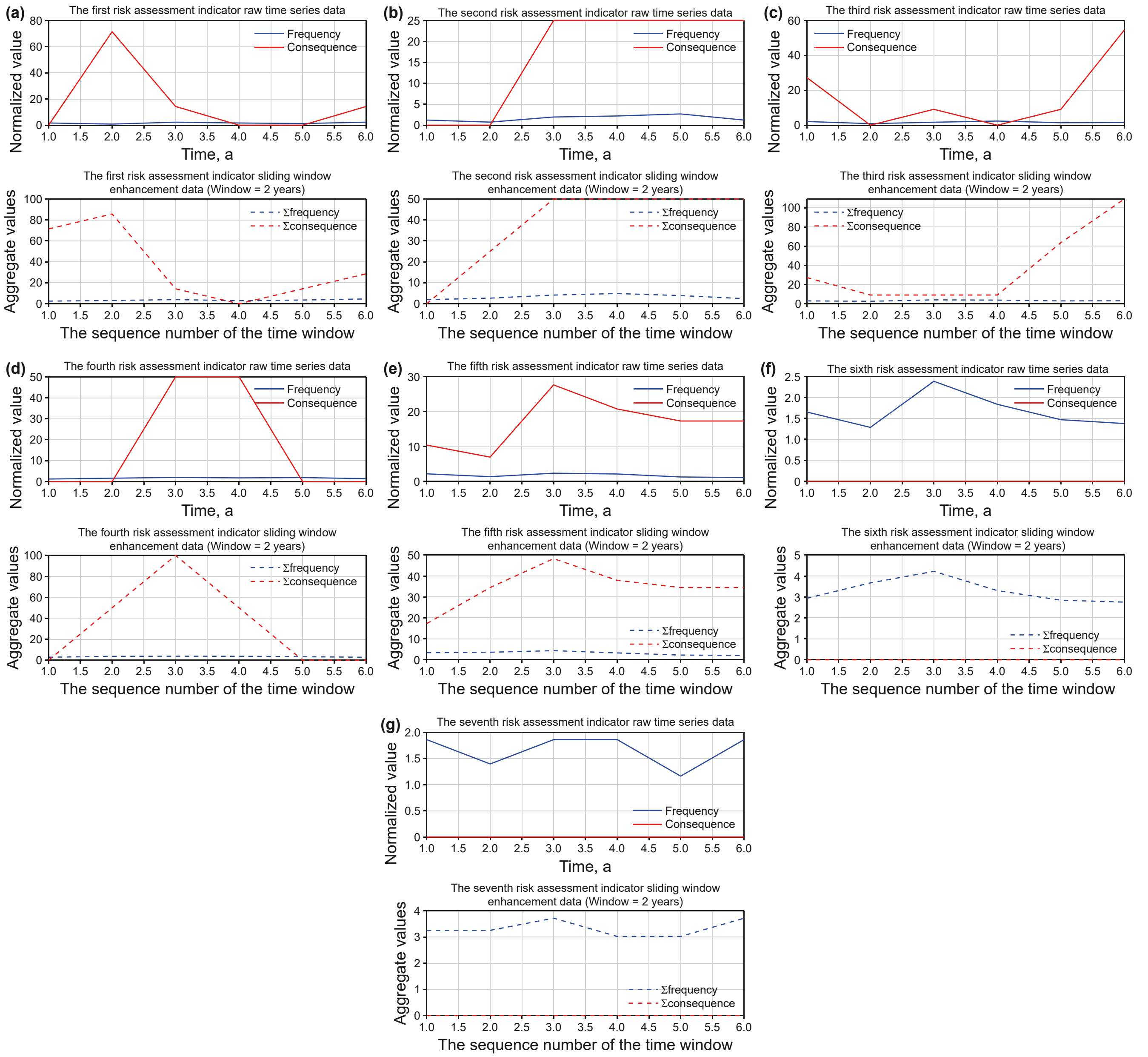

Fig. 8. Data enhancement. **(a)** Damage by operator, **(b)** incorrect equipment operation, **(c)** incorrect installation, **(d)** incorrect valve position, **(e)** other incorrect operation, **(f)** overfill of tank, **(g)** pipeline overpressured.

Table 7
The temporal stability and risk differentiation of the model before and after data enhancement.

	Before enhancement	After enhancement
Temporal stability	0.7726	0.7983
Risk differentiation	2.6500	3.0900

Table 8
The reduction rate of weight variance before and after data enhancement.

Risk assessment indicators	Frequency	Casualty figures
Damage by operator	56.90%	60.84%
Incorrect equipment operation	39.06%	34.38%
Incorrect installation	71.29%	6.06%
Incorrect valve position	50.77%	37.50%
Other incorrect operation	37.22%	54.01%
Overfill of tank	54.47%	–
Pipeline overpressured	73.62%	–

reflected by positive variance reduction rates), leading to notable improvements in temporal stability (an increase of 3.3%) and risk differentiation (an elevation of 16.6%).

As shown in Table 9, the enhanced indicator data are input into the corresponding dynamic membership functions to generate membership degrees for each time period, which are then used to construct a three-dimensional fuzzy matrix. The matrix represents the temporal evolution of risk levels for each indicator. Darker colors correspond to higher risk levels. Based on risk classification criteria, five risk levels are defined: extremely low, medium, high, and extremely high, with the corresponding intervals specified as: $(0, 0.2]$, $(0.2, 0.4]$, $(0.4, 0.6]$, $(0.6, 0.8]$, $(0.8, 1.0]$.

Table 9
The membership degree of the risk assessment indicators at different time periods.

Risk assessment indicators	The membership degree at the six time periods					
Damage by operator	0.9946	0.9992	0.9754	0.4913	0.9640	0.9976
Incorrect equipment operation	0.3968	0.9998	1	1	1	1
Incorrect installation	1	1	1	1	1	1
Incorrect valve position	0.6973	1	1	1	0.6973	0.6973
Other incorrect operation	1	1	1	1	1	1
Overfill of tank	0.5	0.5	0.5	0.5	0.5	0.5
Pipeline overpressured	0.3320	0.3320	0.3230	0.3320	0.3320	0.3320

Based on Table 9, a heatmap of the three-dimensional fuzzy matrix is generated, as shown in Fig. 9.

In Fig. 9, the three axes of the matrix correspond to time periods, risk assessment indicators, and associated risk levels, respectively. A color scale is employed to quantitatively represent risk intensity. The color gradient denotes the membership degree. The corresponding risk level is derived from the membership degree and the established membership intervals. To better illustrate the temporal evolution of individual risk factors, the matrix is decomposed into a set of indicator-specific matrices, as shown in Fig. 10.

In Fig. 10(a), damage by operator remains at an extremely high risk level during the first three time periods. Between the third and fourth periods, its risk level declines to medium. However, during the fifth and sixth periods, the risk level increases again and ultimately returns to the extremely high category. Several indicators exhibit pronounced temporal volatility, such as damage by operator and incorrect valve position, whereas others, including other incorrect operations and tank overfilling, maintain relatively stable risk levels. These findings indicate that certain indicators are more sensitive to external disturbances.

(4) Risk priority calculation

By integrating the cloud model with the improved TOPSIS algorithm, the comprehensive closeness degrees of the indicators are obtained from the corresponding membership degrees (Table 9), thus establishing a risk priority ranking. The resulting comprehensive closeness degrees are 0.3810, 0.3854, 0.3354, 0.4089, 0.3354, 0.5988, and 0.6646, as illustrated in Fig. 11.

A smaller comprehensive closeness degree indicates a higher risk priority. Among these indicators, other incorrect operation exhibits the highest risk priority, underscoring its dominant influence in risk assessment.

4.2. Parameter sensitivity analysis

To assess the robustness of the DW-TDFE model in calculating dynamic weights, a sensitivity analysis is performed on the noise expansion factor β. This factor regulates the magnitude of Gaussian noise, thereby influencing weight stability. First, the variance of the initial weights serves as the reference variance. Then, the variance of the dynamic weights is computed under varying values of β. The absolute deviation between the two variances is used to determine the optimal β. The results are shown in Table 10.

When $\beta = 1.2$, the variance is closest to the target variance and remains relatively low. This indicates that, at this setting, the dynamic weights can accurately reflect actual fluctuations. A smaller variance indicates reduced volatility and enhanced stability. Therefore, 1.2 is determined as the optimal value of β.

4.3. Model performance analysis

Based on the dynamic weights, simulation data incorporating Gaussian noise are generated to emulate real-time operational

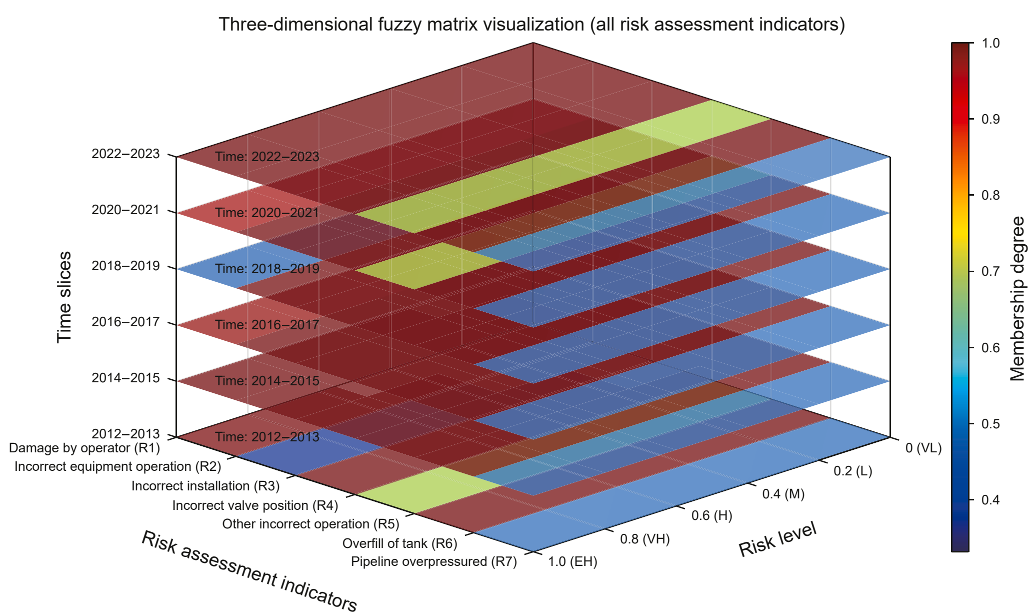

Fig. 9. The heatmap of the three-dimensional fuzzy matrix.

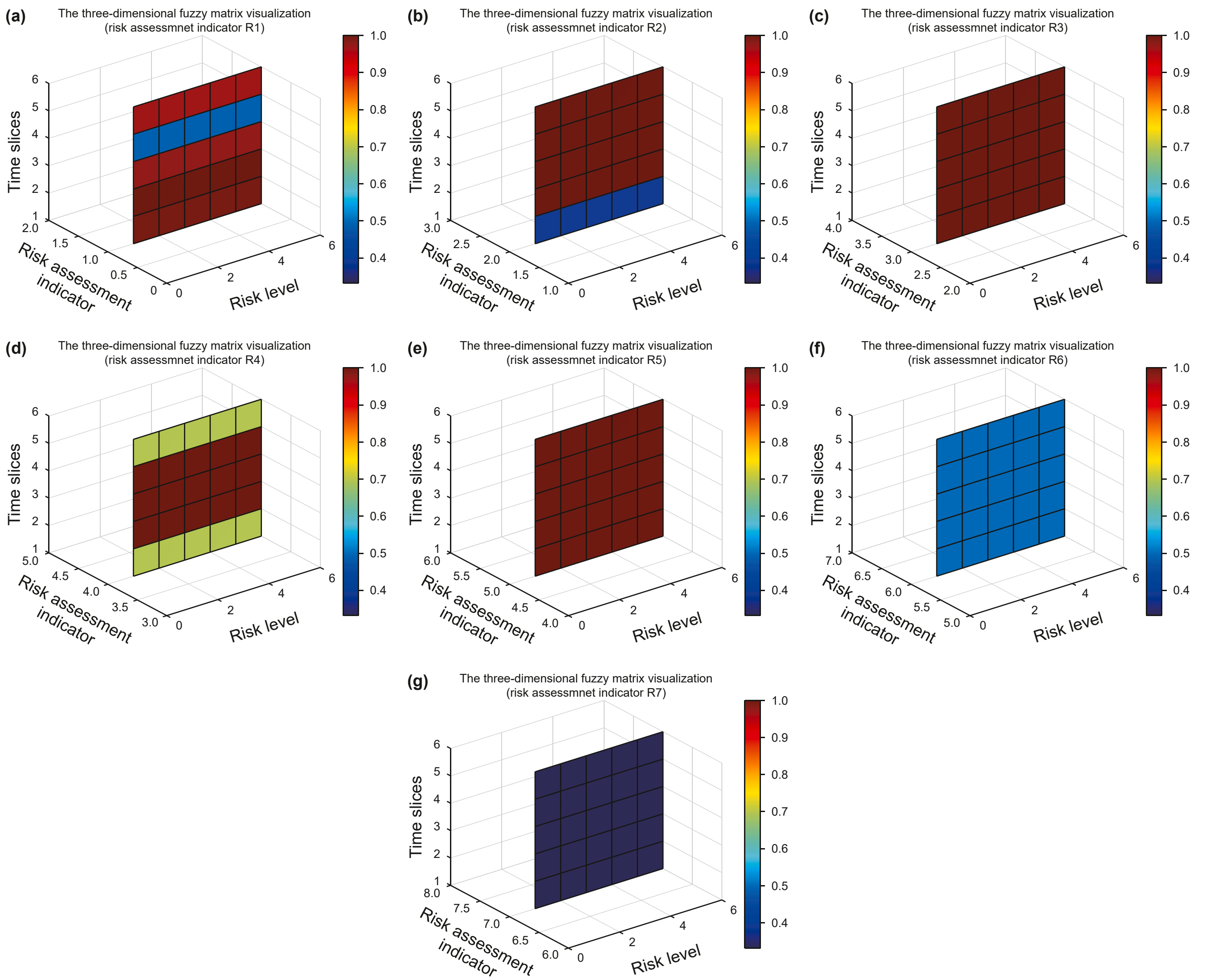

Fig. 10. Indicator-specific matrices. **(a)** Damage by operator, **(b)** incorrect equipment operation, **(c)** incorrect installation, **(d)** incorrect valve position, **(e)** other incorrect operation, **(f)** overfill of tank, **(g)** pipeline overpressured.

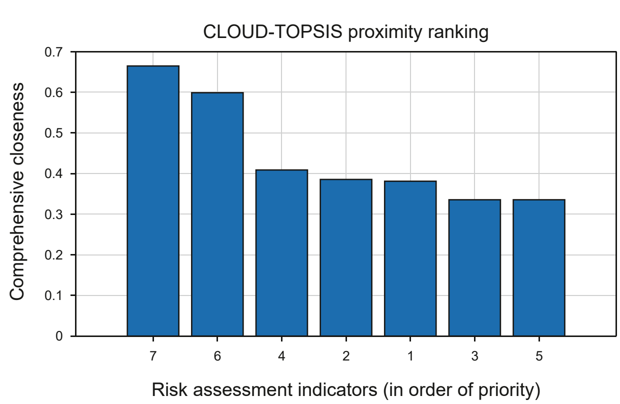

Fig. 11. The comprehensive closeness degree.

Table 10
The absolute value of the difference between the dynamic weight variance and the initial weight variance of the noise expansion factors β.

Noise expansion factor β	Dynamic weight variance	Initial weight variance	Absolute value of the difference
0.8	0.0024	0.0031	0.0007
1.0	0.0025	0.0031	0.0006
1.2	0.0028	0.0031	0.0003
1.5	0.0040	0.0031	0.0009
1.8	0.0027	0.0031	0.0004
2.0	0.0023	0.0031	0.0008

conditions, evaluating the performance of the DW-TDFE model. Sampling is conducted at 3-h intervals over a 24-h cycle.

In Fig. 12, the black dashed lines represent the initial indicator weights, the blue lines correspond to abnormal data generated by human operational errors, and the red lines denote the DW-TDFE model's responses to these abnormalities. As shown in Table 11, under abnormal data conditions, the DW-TDFE model achieves mean accuracy, precision, and recall rates exceeding 90%, demonstrating its outstanding performance. Moreover, the dynamic weight adjustment mechanism effectively balances noise suppression and sensitivity to risk variation, thereby ensuring

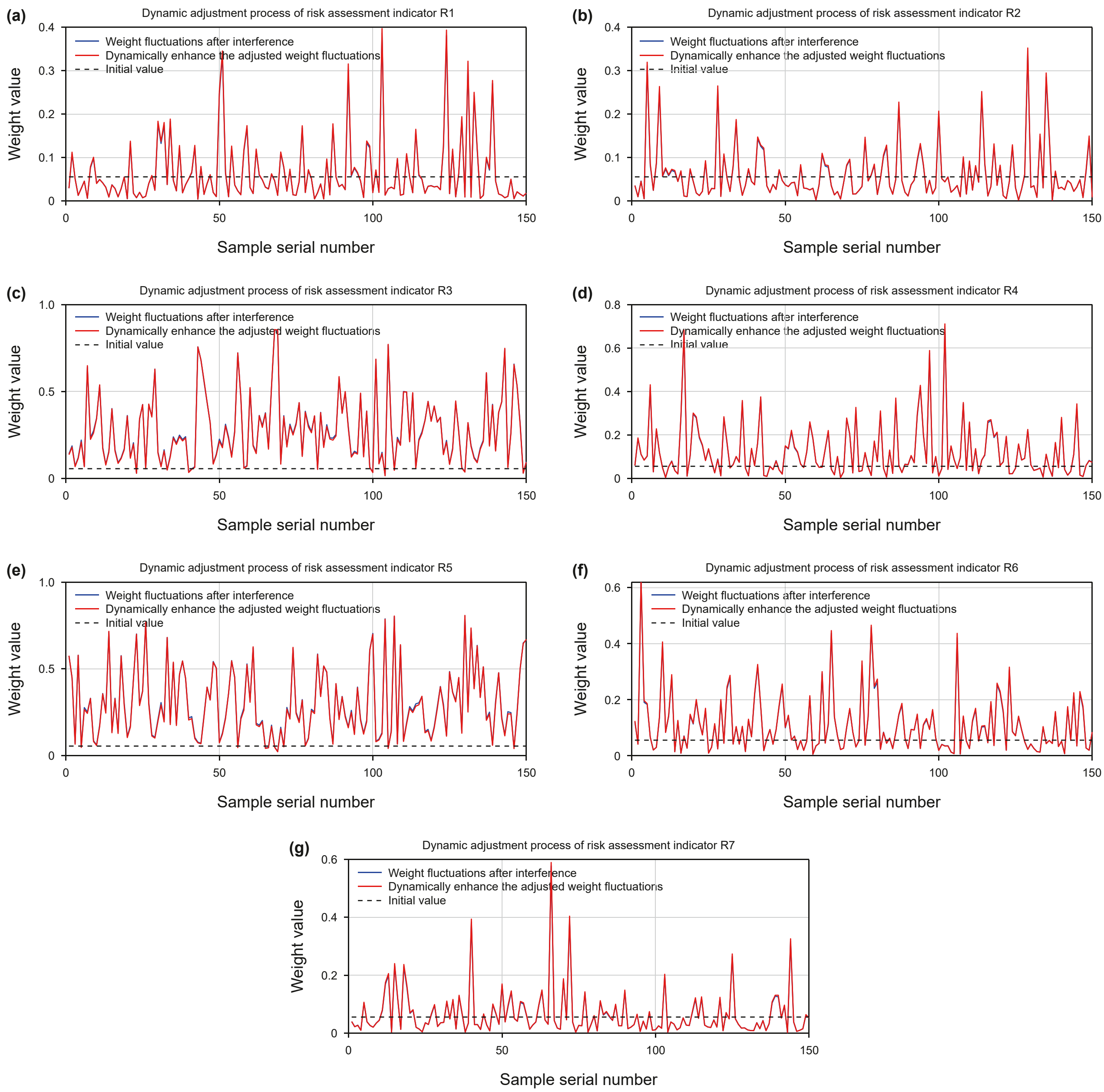

Fig. 12. Dynamic cloud weight adjustment. **(a)** Damage by operator, **(b)** incorrect equipment operation, **(c)** incorrect installation operation, **(d)** incorrect valve position, **(e)** other incorrect operation, **(f)** overfill of tank, **(g)** pipeline overpressured.

reliable early warnings for increasing risk levels. Meanwhile, the DW-TDFE model identifies specific risk assessment indicators associated with abnormalities by highlighting those with significantly increased weights (Fig. 13). The results in Figs. 12 and 13 and Table 11 verify that the DW-TDFE model can accurately respond to abnormal signals and localize key risk factors, enabling real-time dynamic monitoring of risk indicators.

The risk level of “damage by operator” decreases from extremely high to medium during the fourth time period (2018–2019) (Fig. 10). This may be attributed to the implementation of the Pipeline Integrity Management Program by PHMSA in 2017, which standardized operational procedures and strengthened regulatory oversight. Consequently, both pipeline accidents and casualties associated with this risk factor declined

Table 11
The performance metrics of the DW-TDFE model.

Performance metrics	Time period								Mean
Accuracy	99.86%	99.43%	99.00%	97.86%	95.57%	93.29%	89.43%	83.79%	94.75%
Precision	100.0%	100.0%	100.0%	99.81%	98.59%	94.13%	86.96%	77.41%	94.61%
Recall	99.63%	98.53%	97.43%	94.68%	89.91%	88.26%	85.69%	82.39%	92.07%

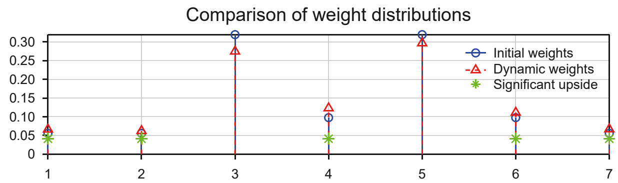

Fig. 13. Indicators with significantly increased weights.

significantly. In contrast, "other incorrect operation" remains at an extremely high risk level. This persistence reflects the broad scope of non-compliant behaviors encompassed by this category. The risk threshold θ for "incorrect installation" is extremely low (Table 6), indicating that even slight deviations during installation can lead to severe consequences. For instance, in 2013, a pipeline rupture in Arkansas, USA, was caused by the misplacement of a pressure detection device. The improper installation prevented accurate pressure monitoring, resulting in overpressure and subsequent rupture. The crude oil leak polluted nearby water sources and caused one fatality. In 2019, a corrosion-induced pipeline failure in California, attributed to improper installation, led to ignition upon exposure to an open flame and resulted in six fatalities. In contrast, the risk level of "overfill of tank" remains low. This is mainly due to its extremely low shape parameters and the typically limited impact of tank overflow incidents. Furthermore, the widespread adoption of modern storage facilities equipped with level sensors and automatic shutdown systems significantly reduces the associated risks. In summary, the DW-TDFE model demonstrates strong practical applicability.

4.4. Comparison of risk assessment models

To evaluate its performance, the DW-TDFE model was compared with four widely used dynamic risk assessment models: the fuzzy-Bayesian bow-tie (FBB) model (Jayan et al., 2021), the dynamic reliability model for subsea pipeline risk assessment under third-party interference (FTFE) (Aulia et al., 2021), the Bayesian network and game theory-based model for third-party damage to oil and gas pipelines (BNGT) (Cui et al., 2020), and the Bayesian network-based safety barrier model for offshore oil and gas systems (BNSB) (Roberto et al., 2020). The FBB model integrates fuzzy logic with Bayesian networks to address uncertainty in pipeline risk assessments. However, it exhibits limited adaptability to real-time data updates. The FTFE model combines dynamic Bayesian networks with finite element analysis to enable risk prediction throughout the entire pipeline lifecycle, but it is associated with high computational complexity. The BNGT model incorporates Bayesian networks and game theory to represent multi-agent interactions in strategic risk scenarios. However, its performance depends heavily on expert judgment. The BNSB model applies Bayesian networks to assess safety barrier failures in offshore environments. Despite its effectiveness in complex settings, it requires large volumes of data.

Four key performance indicators were adopted for model comparison from longitudinal and cross-sectional perspectives: temporal stability, risk differentiation, historical trend fitting, and risk priority ranking. Temporal stability reflects the model's robustness and consistency over time. Risk differentiation measures its ability to distinguish between varying levels of risk among indicators. Historical trend fitting evaluates how well the model reproduces observed risk evolution. Risk priority ranking measures the model's effectiveness in identifying and ordering critical risk factors for decision-making.

Using real-world data, the performance of all models in terms of temporal stability, risk differentiation, and historical trend fitting is summarized in Table 12. The results of risk priority ranking are shown in Table 13.

The DW-TDFE model demonstrates superior performance. For temporal stability, the DW-TDFE model outperforms the FBB, BNGT, and BNSB models, demonstrating strong robustness and reliability under time-varying data conditions. In risk differentiation, the DW-TDFE model achieves the highest performance score ($3.0900 > 2.8400 > 1.7237 > 1.0502 > 0.9396$), indicating its enhanced capability to discriminate effectively among risk levels. Regarding historical trend fitting, the DW-TDFE model ranks second among the five models, reflecting its strong capability to capture risk evolution trends.

As shown in Table 13, "other incorrect operation" and "incorrect installation" are consistently identified as the highest-risk indicators, whereas "pipeline overpressure" is assigned the lowest priority. The five models exhibit a high degree of consistency in their risk-ranking outcomes. Kendall's tau correlation coefficients between the DW-TDFE model and the four benchmark models are 1, 0.714, 0.810, and 0.781, respectively, yielding an average correlation coefficient of 0.768. These results demonstrate strong agreement between the DW-TDFE model and existing approaches, thus confirming the credibility and reliability of the proposed model in dynamic risk assessment settings.

In conclusion, the DW-TDFE model provides a robust methodological framework for dynamic risk evaluation, supported by its superior temporal stability, enhanced risk discrimination capability, and reliable trend-tracking performance.

Table 12
The temporal stability, risk differentiation, and historical trend fitting of the five models.

Risk assessment model	Temporal stability	Risk differentiation	Historical trend fitting	References
DW-TDFE	0.7983	3.0900	0.8286	
FBB	0.7975	2.8400	0.8142	Jayan et al. (2021)
FTFE	0.8000	0.9396	0.8329	Aulia et al. (2021)
BNGT	0.5191	1.7237	–	Cui et al. (2020)
BNSB	0.3151	1.0502	0.8000	Roberto et al. (2020)

Table 13
The risk priority ranking results.

Risk assessment indicator	DW-TDFE	FBB	FTFE	BNGT	BNSB
Damage by operator	3	3	4	4	4
Incorrect equipment operation	4	4	6	5	5
Incorrect installation	2	2	2	2	2
Incorrect valve position	5	5	3	3	3
Other incorrect operation	1	1	1	1	1
Overfill of tank	6	6	5	6	6
Pipeline overpressured	7	7	7	7	6
References		Jayan et al. (2021)	Jayan et al. (2021)	Cui et al. (2020)	Roberto et al. (2020)

5. Conclusion

Risk assessment is crucial for ensuring the safe operation of oil and gas pipelines. To address the limitations of conventional methods in handling uncertainty, particularly that arising from human operational errors, this study proposed the DW-TDFE model. The model incorporated a dynamic weight adjustment matrix and utilized a hyperbolic tangent function to mitigate weight fluctuations. Gaussian noise was further introduced to simulate operational disturbances in real-world pipeline systems. Parameter optimization of the dynamic membership functions was achieved using a gradient descent algorithm. The collected data were enhanced to construct a three-dimensional fuzzy matrix, capturing the time-varying risk levels of the indicators. The comprehensive closeness degree of each indicator was calculated and used for priority ranking.

The results demonstrate that the DW-TDFE model can effectively capture weight fluctuations induced by such disturbances, providing timely feedback to risk managers and supporting the formulation of appropriate risk mitigation strategies. Comparative evaluations against four widely adopted dynamic risk assessment models further confirm the superior performance of the DW-TDFE model in terms of temporal stability, risk differentiation, and historical trend fitting. These findings indicate that the DW-TDFE model exhibits strong robustness and noise tolerance, making it suitable for complex risk assessment scenarios involving multiple risk factors.

By appropriately adjusting the risk indicator system, the model can be tailored to meet varying risk assessment requirements. When applied to the safety evaluation of chemical production processes, the DW-TDFE model allows the substitution of the risk assessment indicator "incorrect operation" with "process parameter deviation", wherein dynamic weights reflect the real-time impact of temperature and pressure sensor errors. Data enhancement techniques are employed to mitigate sensor noise, generating a risk level heatmap. In the context of surgical risk assessment, mirror symmetric padding is introduced to augment limited sample datasets, thereby enhancing the model's capability to capture temporal trends. By integrating cloud models to quantify the inherent uncertainty and fuzziness associated with surgical errors, the DW-TDFE framework achieves effective risk assessment.

The proposed DW-TDFE model provides robust support for risk management decision-making in engineering practice by dynamically assessing risk factors associated with human operational errors in oil and gas pipelines. The risk priority ranking results generated by the DW-TDFE model enable risk managers to identify critical risk factors and formulate targeted safety interventions. For indicators with high-risk priority, it is recommended to prioritize equipment maintenance or replacement and to enhance specialized training for frontline operators to improve operational reliability.

The model's dynamic weight adjustment mechanism allows for the timely detection of abnormal signals. When the weight of a specific risk assessment indicator increases abnormally, the system automatically issues an alert, prompting on-site personnel to inspect the relevant equipment immediately. Furthermore, by incorporating enhanced data, the DW-TDFE model captures medium-to long-term risk evolution patterns, enabling the identification of cyclical risks and the formulation of seasonal prevention and control strategies. Through continuous updating of input data, the model iteratively refines risk response strategies. The three-dimensional fuzzy matrix derived from the DW-TDFE model facilitates the identification of high-risk periods, enabling rapid fault localization and reducing response times. This supports the dynamic optimization of inspection schedules: during high-risk periods, inspection frequency should be increased or supplemented with remote monitoring, whereas during low-risk periods, inspection efforts can be reduced and reallocated to other high-risk areas.

Overall, the DW-TDFE model exhibits excellent temporal stability, risk differentiation, and historical trend fitting, ensuring high assessment accuracy and long-term reliability. It supports risk trend analysis and cross-departmental collaborative decision-making, thereby improving the overall safety of pipeline operations. Moreover, the model's universal framework is adaptable to other high-risk industries, such as chemical processing and power generation, providing a comprehensive solution for dynamic risk management in complex systems.

Despite its effectiveness, the model has several limitations. Most notably, it relies heavily on historical accident data. Future research would incorporate transfer learning and multi-source data fusion to identify emerging risks and adapt to changing operational environments. Additionally, future work will aim to reduce computational complexity through algorithmic optimization, thereby enabling deployment on embedded platforms for real-time early warning applications. Finally, the framework will be extended to additional high-risk industries by incorporating dedicated human error modeling.

CRediT authorship contribution statement

Xue-Qiang Qu: Writing – original draft. **Jiang-Tao Cao:** Writing – review & editing. **Tao-Yan Zhao:** Writing – review & editing. **Zhe Kan:** Methodology.

Declaration of competing interest

The authors declare that they have no known competing financial interests or personal relationships that could have appeared to influence the work reported in this paper.

Acknowledgments

This work was supported by the Liaoning Provincial Science and Technology Joint Plan Project (Key Research and Development Project) (Grant No. 2025JH2/101800046), the National Local Joint Engineering Laboratory for Optimization of Petrochemical Process Operation and Energy saving Technology (Grant No. LJ232410148002), the Innovation Team Project of the Educational Department of Liaoning Province (Grant No. LJ222410148036), the Liaoning Province Applied Basic Research Program Project (Grant No. 2023JH26/10300013), the Program for Scientific Research Fund Project of the Educational Department of Liaoning Province of China (Grant No. LJ212410148061), and the National and Local Joint Engineering Laboratory for Process Operation Optimization and Energy-saving Technology in Petrochemical Industry (Grant No. LJ232510148001).

References

Aulia, R., Tan, H., Sriramula, S., 2021. Dynamic reliability model for subsea pipeline risk assessment due to third-party interference. J. Pipeline Sci. Eng. 1 (3), 277–289. https://doi.org/10.3850/978-981-11-2724-3_0497-cd.

Ba, Z.N., Wang, Y., Fu, J.S., et al., 2021. Corrosion risk assessment model of gas pipeline based on improved AHP and its engineering application. Arab J. Sci. Eng. 47 (9), 1–19. https://doi.org/10.1007/s13369-021-05496-9.

Bakhtiari, S., Najafi, M.R., Goda, K., et al., 2025. A dynamic Bayesian network approach to characterize multi-hazard risks and resilience in interconnected critical infrastructures. Reliab. Eng. Syst. Saf. 257, 110815. https://doi.org/10.1016/j.ress.2025.110815.

Cui, Y., Quddus, N., Mashuga, C.V., 2020. Bayesian network and game theory risk assessment model for third-party damage to oil and gas pipelines. Proc. Saf. Environ. 134, 178–188. https://doi.org/10.1016/j.psep.2019.11.038.

Díaz, H., Teixeira, A.P., Soares, C.G., 2022. Application of monte carlo and fuzzy analytic hierarchy processes for ranking floating wind farm locations. Ocean. Eng. 245, 110453. https://doi.org/10.1016/j.oceaneng.2021.110453.

Fahd, K., Miah, S.J., 2023. Effectiveness of data augmentation to predict students at risk using deep learning algorithms. Soc. Netw. Anal. Min. 13 (1), 113. https://doi.org/10.1007/s13278-023-01117-5.

Fu, Z., Gong, A., Wan, J., et al., 2025. Forest fire risk assessment model optimized by stochastic average gradient descent. Ecol. Indic. 170, 113006. https://doi.org/10.1016/j.ecolind.2024.113006.

Graham, K.J., Kinney, G.F., 1980. A practical safety analysis system for hazards control. J. Saf. Res. 12 (1), 13–20. https://trid.trb.org/View/154356.

Gul, M., Lo, H.W., Yucesan, M., 2021. Fermatean fuzzy TOPSIS-based approach for occupational risk assessment in manufacturing. Complex Intell. Syst. 7 (5), 2635–2653. https://doi.org/10.1007/s40747-021-00417-7.

Jayan, J.T., Muthukumar, K., Renjith, V.R., et al., 2021. The risk assessment of a crude oil pipeline using fuzzy and bayesian based bow-tie analysis. J. Eng. Res.-Kuwait 9. https://doi.org/10.36909/jer.icmmm.12399.

Koulinas, G.K., Demesouka, O.E., Sidas, K.A., et al., 2021. A TOPSIS—Risk matrix and monte carlo expert system for risk assessment in engineering projects. Sustain. Basel 13 (20), 11277. https://doi.org/10.3390/su132011277.

Lawal, S.L., Afolalu, S.A., 2024. Human factors in asset integrity: analyzing the role of human error in oil and gas incidents. In: 2024 International Conference on Science, Engineering and Business for Driving Sustainable Development Goals (SEB4SDG), pp. 1–8. https://doi.org/10.1109/SEB4SDG60871.2024.10630418.

Li, X., Ran, Y., Zhang, G., et al., 2020. A failure mode and risk assessment method based on cloud model. J. Intell. Manuf. 31, 1339–1352. https://doi.org/10.1007/s10845-019-01513-9.

Lin, C.J., Zhang, M., Li, L.P., et al., 2020. Risk assessment of tunnel construction based on improved cloud model. J. Perform. Constr. Facil. 34 (3), 04020028. https://doi.org/10.1061/(asce)cf.1943-5509.0001421.

Lu, C., Li, S., Xu, N., et al., 2025. Hybrid-driven risk assessment methodology for coal and gas outburst: integration of complex network, disaster mechanism, and multi-level fusion modeling. Proc. Saf. Environ., 107226 https://doi.org/10.1016/j.psep.2025.107226.

Lu, C., Li, S., Xu, N., et al., 2025. Research on AI-driven complex network and management system of coal and gas outburst accident. J. Saf. Environ. 2 (1), 32–44. https://doi.org/10.1016/j.jsasus.2025.02.002.

Lu, X.R., 2018. Review and analysis of the 2018 edition of ISO 31000 "Risk management guidelines". China J. Comm. vol. 20, 165–166. https://doi.org/10.19699/j.cnki.issn2096-0298.2018.20.165 (in Chinese).

Pathan, A.I., Girish, A.P., Said, S., et al., 2022. AHP and TOPSIS based flood risk assessment-a case study of the Navsari city, Gujarat, India. Environ. Monit. Assess. 194 (7), 509. https://doi.org/10.1007/s10661-022-10111-x.

Pezoulas, V.C., Grigoriadis, G.I., Gkois, G., et al., 2021. A computational pipeline for data augmentation towards the improvement of disease classification and risk stratification models: a case study in two clinical domains. Comput. Biol. Med. 134, 104520. https://doi.org/10.1016/j.compbiomed.2021.104520.

Pipeline and Hazardous Materials Safety Administration, 2023. https://www.phmsa.dot.gov.

Riela, P.M., 2022. Data Augmentation and Machine Learning for Risk Assessment in Healthcare Associated Infections. https://tesidottorato.depositolegale.it/handle/20.500.14242/72466.

Roberto, B., Shenae, L., Daniel, M., et al., 2020. Dynamic assessment of safety barriers preventing escalation in offshore oil&gas. Saf. Sci. 121, 319–330. https://doi.org/10.1016/j.ssci.2019.09.011.

Saffarian, S., Mahmoudi, A., Shafiee, M., et al., 2020. Measuring the effectiveness of AHP and fuzzy AHP models in environmental risk assessment of a gas power plant. Hum. Ecol. Risk Assess. 27 (5), 1227–1241. https://doi.org/10.1080/10807039.2020.1816809.

Wang, W., Wang, Y., Fan, S., et al., 2023. A complex spherical fuzzy CRADIS method based fine-Kinney framework for occupational risk evaluation in natural gas pipeline construction. J. Pipeline Sci. Eng. 220, 111246. https://doi.org/10.1016/j.petrol.2022.111246.

Wang, X., Duan, Q., 2019. Improved AHP–TOPSIS model for the comprehensive risk evaluation of oil and gas pipelines. Pet. Sci. 16 (6), 1479–1492. https://doi.org/10.1007/s12182-019-00365-5.

Yu, J.X., Chen, H.C., Wu, S.B., et al., 2021. A novel risk matrix approach based on cloud model for risk assessment under uncertainty. IEEE Access 9, 27884–27896. https://doi.org/10.1109/access.2021.3058392.

Zhan, Y., Zhang, Y., Zhang, J., et al., 2025. Risk assessment of land subsidence in Shanghai municipality based on AHP and EWM. Sci. Rep. 15 (1), 7339. https://doi.org/10.1038/s41598-025-91109-6.